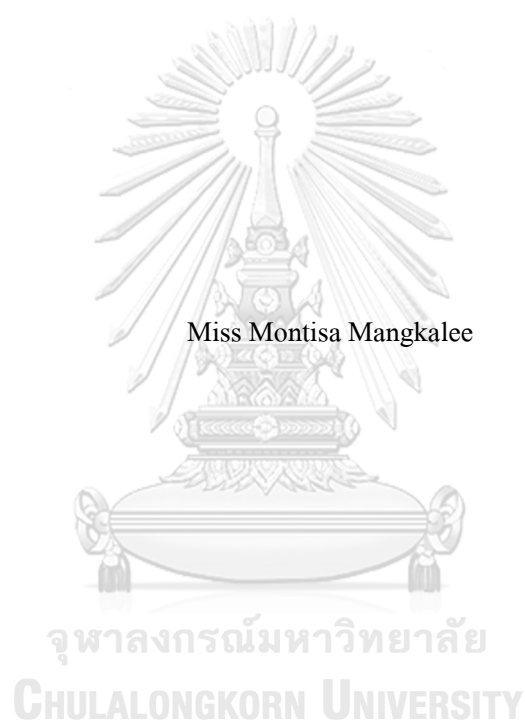


KINETIC MECHANISM OF DIMETHYLSULFONE MONOOXYGENASE AND ITS
IMMOBILIZED MAGNETIC NANOPARTICLES



A Dissertation Submitted in Partial Fulfillment of the Requirements
for the Degree of Doctor of Philosophy in Chemistry

Department of Chemistry

Faculty Of Science

Chulalongkorn University

Academic Year 2023

กลไกทางจลนศาสตร์ของเอนไซม์โคเมทิลซัลโฟนโมโนออกซีจีเนสและการตรึงเอนไซม์บน
อนุภาคแม่เหล็กระดับนาโนเมตร



วิทยานิพนธ์นี้เป็นส่วนหนึ่งของการศึกษาตามหลักสูตรปริญญาวิทยาศาสตรดุษฎีบัณฑิต
สาขาวิชาเคมี ภาควิชาเคมี
คณะวิทยาศาสตร์ จุฬาลงกรณ์มหาวิทยาลัย
ปีการศึกษา 2566

มณฑิสา มังคะลี : กลไกทางจลนศาสตร์ของเอนไซม์ไดเมทิลซัลโฟนโมโนออกซิจีเนส และการตรึงเอนไซม์บนอนุภาคแม่เหล็กระดับนาโนเมตร. (KINETIC MECHANISM OF DIMETHYLSULFONE MONOOXYGENASE AND ITS IMMOBILIZED MAGNETIC NANOPARTICLES) อ.ที่ปรึกษาหลัก : ผศ. ดร.นำพล อินสิน, อ.ที่ปรึกษา ร่วม : รศ. ทพ. ดร.จิรัชย์ สุจริตกุล

Dimethyl sulfone (DMSO₂) monooxygenase เป็นเอนไซม์ที่เร่งปฏิกิริยา monooxygenation จากออกซิเจนไปสู่สารตั้งต้น dimethyl sulfone การ oxygenation นำไปสู่การกำจัดคาร์บอนหนึ่งตัวจากสารตั้งต้นและเกิด methanesulfinat และฟอร์มัลดีไฮด์เป็น product ระบบการปฏิกิริยามีเอนไซม์สองตัวเป็นตัวประกอบ ได้แก่ Reductase (DMSR) และ Monooxygenase (DMSMO) DMSR เป็นฟลาวอโปรตีนที่มี FMN (ฟลาวินโมโนนิวคลีโอไทด์) เป็น co-factor DMSR มีบทบาทสำคัญในการสร้าง FMN ที่โดน reduced โดยใช้ NADH เป็นตัวให้อิเล็กตรอน DMSMO มีหน้าที่สำหรับ monooxygenation เพื่อรวมอะตอมของออกซิเจนเข้ากับ DMSO₂ เกิดผลเป็น methanesulfinat และฟอร์มัลดีไฮด์ อย่างไรก็ตาม กลไกการเกิดปฏิกิริยาของเอนไซม์ทั้งสองในระบบสององค์ประกอบนี้ยังไม่เคยได้รับการวิจัย การศึกษาวิจัยนี้ได้อธิบาย kinetic mechanism ของเอนไซม์โดยใช้ rapid kinetic ซึ่งทำการวิจัยโดยใช้เครื่อง stopped-flow spectrophotometer ผลปฏิกิริยากับ O₂ ไม่พบตัวกลางปฏิกิริยา ดังนั้น H₂O₂ จึงน่าจะเป็นสารให้ออกซิเจนแก่ DMSO₂ ซึ่งได้รับการยืนยันจากผลการวิจัยนี้ Rapid quenched-flow ถูกใช้เพื่อหาค่าคงที่อัตราของ monooxygenation ซึ่งมีค่าใกล้เคียงกับค่าคงที่ของการ oxidize flavin ซึ่งบ่งชี้ว่า monooxygenation ของ H₂O₂ ที่ทำปฏิกิริยากับ DMSO₂ เร็วมาก และฟลาวินออกซิเดชันกลายเป็น rate-limiting step การวิจัยนี้เป็นวิจัยแรกที่น่าเสนอกลไกสมดุลของทั้งสององค์ประกอบโดยใช้ rapid kinetic และวิธีการตรวจจับ methanesulfinat โดยใช้ LC-MS เอนไซม์ทั้งสองได้โดนตรึงกับอนุภาคแม่เหล็กระดับนาโนเมตร (CoFe₂O₄@SiO₂ – Ni/NTA) เพื่อเพิ่มประสิทธิภาพของเอนไซม์ในสิ่งแวดล้อมต่างๆและเพิ่มความสามารถในการแยกตัวเอนไซม์ออกจากผลิตภัณฑ์และนำกลับมาใช้ได้ อีกกระบวนการย่อยสลาย DMSO₂ อาจนำไปสู่การประยุกต์ใช้ในการบำบัดน้ำเสียที่มีสารประกอบกำมะถันอันตราย

สาขาวิชา เคมี
ปีการศึกษา 2566

ลายมือชื่อนิสิต
ลายมือชื่อ อ.ที่ปรึกษาหลัก
ลายมือชื่อ อ.ที่ปรึกษา ร่วม

6072885623 : MAJOR CHEMISTRY

KEYWORD: two-component flavin-dependent enzyme, dimethyl sulfone, dimethyl sulfone monooxygenase, co-immobilization, magnetic nanoparticles

Montisa Mangkalee : KINETIC MECHANISM OF DIMETHYLSULFONE MONOOXYGENASE AND ITS IMMOBILIZED MAGNETIC NANOPARTICLES.

Advisor: Asst. Prof. Dr. NUMPON INSIN, Ph.D. Co-advisor: Assoc. Prof. Dr. JEERUS SUCHARITAKUL, D.D.S., Ph.D.

The dimethyl sulfone monooxygenase system is a two-component flavoprotein catalyzing the monooxygenation of dimethyl sulfone (DMSO₂) by oxidative cleavage producing methanesulfinate and formaldehyde. The reductase component (DMSR) is a flavoprotein with FMN as a cofactor catalyzing flavin reduction using NADH. The oxygenase (DMSMO) uses reduced flavin from the reductase and oxygen for substrate monooxygenation. DMSMO can bind to FMN and FMNH⁻ with a K_d of $17.4 \pm 0.9 \mu\text{M}$ and $4.08 \pm 0.8 \text{ mM}$, respectively. The binding of FMN to DMSMO is required prior to binding DMSO₂. Substituting reduced DMSR with FMNH⁻ demonstrated the same oxidation kinetics, indicating that FMNH⁻ from DMSR was transferred to DMSMO. The oxidation of FMNH⁻:DMSMO, with and without DMSO₂ did not generate any flavin adducts for monooxygenation. Therefore, H₂O₂ is likely to be the reactive agent to attack the substrate. The H₂O₂ assay results demonstrated production of H₂O₂ from the oxidation of FMNH⁻:DMSMO, whereas H₂O₂ was not detected in the presence of DMSO₂, confirming H₂O₂ utilization. The rate constant for methanesulfinate formation determined from rapid-quenched flow and the rate constant for flavin oxidation were similar, indicating that H₂O₂ rapidly reacts with dimethyl sulfone. Both enzymes have been co-immobilized onto Ni-NTA functionalized magnetic nanoparticles (CoFe₂O₄@SiO₂-Ni/NTA) to improve enzyme stability in different environments and enable the enzymes to be recovered for reuse.

Field of Study: Chemistry

Student's Signature

Academic Year: 2023

Advisor's Signature

Co-advisor's Signature

ACKNOWLEDGEMENTS

I would like to acknowledge The Royal Golden Jubilee Scholarship for their financial support. It has been an honor to be part of the RGJ. PHD scholarship program.

An immense thank you to my PhD supervisors, Dr. Numpon Insin and Dr. Jeerus Sucharitakul. Support and guidance throughout the project from you all has been invaluable. Thank you to all the academics who helped me get to this stage.

It has been an amazing experience working between different research groups across different Departments and University, thanks to everyone from the Nanochem CU, Department of Chemistry, Faculty of Science and Department of Biochemistry, Faculty of Dentistry, Chulalongkorn University groups I've worked with and from whom I've learned so much. Thank you to Dr. Pimchai Chaiyen research group at Vidyasirimedhi Institute of Science and Technology and Dr. Rachanok group at Mahidol University for providing me with useful equipment, advice and supports.

Thanks of course to my family for being so supportive and helping me every step of the way.



Montisa Mangkalee

TABLE OF CONTENTS

	Page
ABSTRACT (THAI).....	iii
ABSTRACT (ENGLISH).....	iv
ACKNOWLEDGEMENTS.....	v
TABLE OF CONTENTS.....	vi
Rationales.....	1
1. Introduction.....	2
1.1 Introduction to Dimethyl sulfone (DMSO).....	2
1.2 The Dimethyl sulfone monooxygenase system.....	3
1.3 Flavin-dependent two-component enzyme.....	4
1.3.1 The flavin dependent monooxygenase.....	5
1.3.2 The flavin dependent reductase.....	6
1.3.3 Flavin transfer mechanism.....	7
1.4 The use of co-immobilized enzymes for wastewater treatment.....	7
1.4.1 Co-immobilization of enzyme.....	7
2. Methodology.....	8
2.1 Mechanism of two-component enzyme: Dimethyl sulphone monooxygenase.....	8
Reagents.....	8
2.2 Co-immobilization of enzymes onto CoFe ₂ O ₄ magnetic nanoparticle.....	19
Reagents.....	19
3. Results.....	21
3.1. Mechanistic study of enzymes.....	21

3.1.1 Enzyme characterization.....	21
3.1.2 Binding of DMSMO to oxidized FMN.....	25
3.1.3 Binding order of FMN and DMSO ₂ to DMSMO to form a ternary complex.....	26
3.1.4 Oxidation of the FMNH ⁻ :DMSMO complex by oxygen.....	31
3.1.5 Binding of monooxygenase to reduced FMN (FMNH ⁻).....	32
3.1.6 Oxidation of the FMNH ⁻ :DMSMO complex in the presence of DMSO ₂	34
3.1.7 Kinetic reduction and oxidation of the reductase component.....	38
3.1.8 The reduced FMN (FMNH ⁻) transfer from the reduced reductase to DMSMO.....	39
3.1.9 Kinetics of the reduced flavin transfer from reduced DMSR to DMSMO.....	41
3.1.10 Methanesulfinate analysis from enzyme multiple and single turnover.....	44
3.1.11 Effect of H ₂ O ₂ on product formation.....	48
3.1.12 Determination of the rate constants for monooxygenation using rapid-quenched flow.....	49
3.1.13 Quantification of hydrogen peroxide from a single-turnover reaction with or without DMSO ₂	52
3.2. Enzyme immobilization.....	54
3.2.1 Ni-NTA/H ₂ N-SiO ₂ @CoFe ₂ O ₄ characterization.....	54
3.2.2 Immobilization of DMSMO and DMSR onto CoFe ₂ O ₄	55
3.3.3 Efficiency of immobilized enzyme.....	56
3.3.4 Stability of immobilized enzyme.....	57
4. Discussion and Conclusion.....	58
4.1 Mechanistic study of Dimethyl sulfone monooxygenase.....	58
4.2 Co-immobilization of DMSMO and DMSR onto Ni-NTA/H ₂ N-SiO ₂ @CoFe ₂ O ₄	63
REFERENCES.....	67

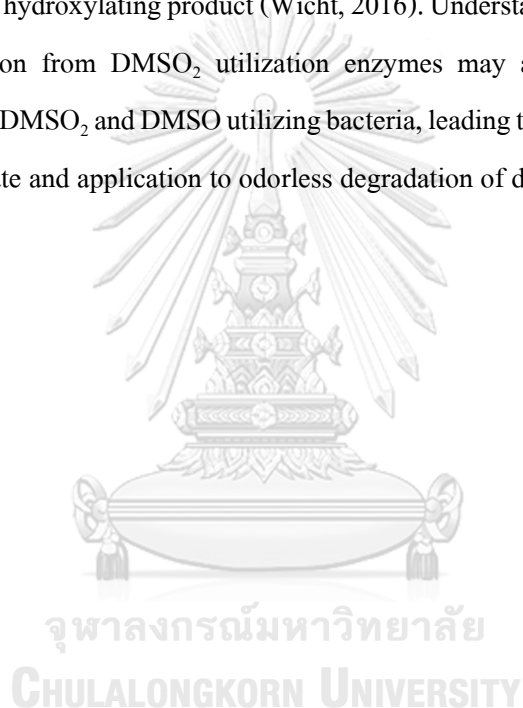
VITA78



จุฬาลงกรณ์มหาวิทยาลัย
CHULALONGKORN UNIVERSITY

Rationales

Dimethyl sulfone monooxygenase (DMSMO) is a flavin-dependent two-component enzyme, which is composed of reductase and oxygenase components. The enzyme is essential for the bacteria sulfur assimilation pathway (Habe et al., 2007). The reductase component functions as a flavin reduction, generating reduced flavin using NADH as an external electron donor. The monooxygenase component accept reduced flavin from the reductase and reacted with molecular oxygen to form an intermediate for the insertion of one oxygen atom into DMSO₂ substrate (Alfieri et al., 2007) to obtain hydroxylating product (Wicht, 2016). Understanding the reaction mechanism and product formation from DMSO₂ utilization enzymes may aid in the elucidation of the metabolism of DMS, DMSO₂ and DMSO utilizing bacteria, leading to insight on the biodegradation route of these substrate and application to odorless degradation of dimethyl sulfoxide (Kino et al., 2004).



1. Introduction

1.1 Introduction to Dimethyl sulfone (DMSO₂)

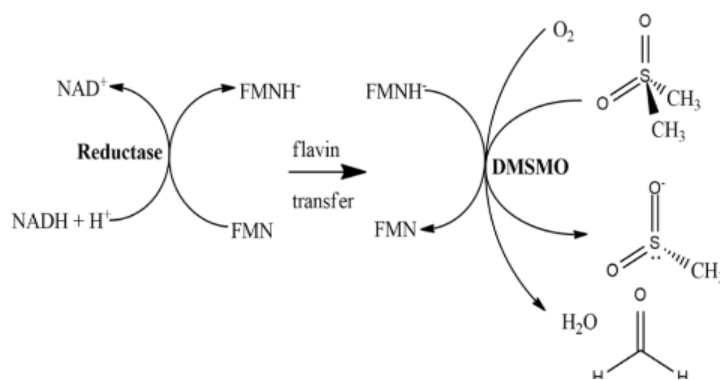
Volatile organic sulfur compounds (VOSCs) have a significant impact on the environment due to their role in cloud condensation, acid precipitation and global warming (Chasteen & Bentley, 2004). The most abundant VOSCs are dimethyl sulfide (DMS) and methanethiol (MT), which are found in large amounts in the marine environment (Bentley & Chasteen, 2004). DMS is the largest natural source of reduced sulfur in the ocean, produced by phytoplankton and dimethyl sulfonium propionate (DMSP). DMS tends to vaporize into the atmosphere due to its insolubility, however, it can be oxidized to dimethyl sulfoxide (DMSO), which is more soluble (Brimblecombe, 2015) and tends to stay in water. The major intermediate of DMS oxidation to sulfate is DMSO and dimethyl sulfone (DMSO₂); these three compounds typically exist in equilibrium in the atmosphere and natural water (Berresheim et al., 1998; Kino et al., 2004). DMSO is widely used in various industries as a dissolving agent, and in washing and rinsing processes, leading to a build-up of the compound and other VOSCs in wastewater (Simó, 1998). DMSO is easily reduced to DMS; both compounds are odorous volatile organic sulfides, which can lead to an odor problem that greatly affects the local population (Kino et al., 2004; Sheng et al., 2008). Therefore, it is favorable for DMSO to be degraded to DMSO₂, a more environmentally friendly and biodegradable compound (Yan et al., 2022). DMSO₂ is an organosulfur compound and serves as a source of sulfur for microorganisms (Hutt, 2018). DMSO₂ is also presented in the human body as a metabolite that can be detected in organs and secretions such as urine, blood and skin (He & Slupsky, 2014). The sources of DMSO₂ in the body are from dietary such as fruits and vegetables that contain methionine (Pearson et al., 1981). Evidence has shown that mice with a high concentration of DMSO₂ have a higher and better function of intestinal microflora used for methionine degradation, showing the importance of DMSO₂ in the metabolic pathway of methionine and the functionality of intestinal microbiota in the body (He & Slupsky, 2014). DMSO₂ is also used in the medical field as a complementary and alternative medicine (CAM), commonly known as methylsulfonylmethane

(MSM), for treatment of arthritis and other inflammatory disorders due to its anti-inflammatory properties (Kim et al., 2009), antioxidant (Beilke et al., 1987) and modulation of immune system (Grimble, 2006). DMSO₂ degradation may cause the equilibrium between DMS, DMSO and DMSO₂ to shift forward, resulting in faster DMS and DMSO degradation (Barnes et al., 2006).

1.2 The Dimethyl sulfone monooxygenase system

Organosulfur compounds are commonly used by microorganisms via several sulfur-regulated desulfurizing enzymes. These enzymes are expressed when prefer sulfur sources (sulfate, cysteine, and thiocyanate) are limited and in sulfate starvation conditions (Kertesz, 2000). Research aimed at the DMS sulfur assimilation pathway of certain bacteria led to an identification of the *sfhG* (DMSMO) enzyme, which involves in the metabolism of DMSO₂. The elucidation of DMSO₂ utilization by bacteria in soil may aid in the understanding of how bacteria metabolized DMS and provide insight on the biodegradation of this compound from exogenous sources (Wicht, 2016).

The dimethyl sulfone monooxygenase (DMSMO) system enzyme is a desulfurizing enzyme that is found in the sulfur assimilation pathway of certain bacteria. The enzyme degrades DMSO₂ to methanesulfinate (Wicht, 2016). The DMSMO system is a two-component flavoprotein, which is composed of a dimethyl sulfone oxygenase component (DMSMO) and a reductase component (DMSR) (**Scheme 1**). DMSR generates reduced flavin using NADH as an external electron donor. DMSMO accepts the reduced flavin from DMSR and reacts with molecular oxygen to insert an oxygen atom into DMSO₂ (Alfieri et al., 2007).



Scheme 1. Reaction mechanism of DMSMO system.

1.3 Flavin-dependent two-component enzyme

Flavin-dependent enzymes or flavoprotein utilize flavin derivatives as cofactors or co-substrates to catalyze the reactions. These flavins are derived from vitamin B2 or riboflavin, commonly found bound to proteins includes flavin adenine dinucleotide (FAD) and flavin mononucleotide (FMN). Approximately 75% of flavoprotein uses FAD while 25% uses FMN and some enzymes can utilize both FMN and FAD. Flavin cofactor are usually noncovalently bound in the active site for majority of the protein, only around 10.8% of known flavoproteins were confirmed to be covalently bound (Macheroux et al., 2011). Flavoprotein can catalyze a wide variety of reactions that involve the transfer of electrons. This versatility was made possible by the ability of the flavin to exist in different redox states (Massey, 2000). Flavoprotein has been used in various applications including as a biocatalyst for the synthesis of various chemical and pharmaceutical industries. It can also be used in bioremediation and biotransformation of waste containing toxic compounds and can be applied as a biosensor or bio-detector for various compounds. In humans, flavoproteins are involved in various cellular activities including metabolite transportation and homeostasis, metabolic transformation, and are also involved in the biosynthesis of essential cofactors and hormones including coenzyme A and Q, hemes, and steroids. Malfunction of these enzymes can cause serious illnesses and diseases (Jortzik et al., 2014; Lienhart et al., 2013). According to their mechanism, flavin-dependent enzymes can be classified into different types including redox neutral flavin-dependent enzymes, dehydrogenase, reductase, oxidase and monooxygenase (Pimviriyakul & Chaiyen, 2020a). Examples of these enzyme can be found in “The Enzyme - Flavin-Dependent Enzymes: Mechanisms, Structures and Applications” (Chenprakhon et al., 2020; Csarman et al., 2020; Ewing et al., 2020; Gadda, 2020; Martin et al., 2020; Phintha et al., 2020; Pimviriyakul & Chaiyen, 2020b; Schmidt & Bornscheuer, 2020; Serrano et al., 2020; Tinikul et al., 2020; Tischler et al., 2020). Flavoproteins classified as monooxygenase enzymes are responsible for catalyzing the cleavage of the oxygen–oxygen bond of dioxygen, inserting one oxygen atom into a substrate, and reducing the other oxygen to water (Massey, 2000).

In general, for a two-component enzyme, genes expressing reductase and monooxygenase enzymes are located in the same operon for ease of utilization (Ellis, 2010). The overall reaction consists of reductive half-reaction to reduce the oxidized flavin cofactor and an oxidative half-reaction where the reduced flavin was cycled back to an oxidized state (Sucharitakul et al., 2014).

1.3.1 The flavin dependent monooxygenase

Three-dimensional structures of several FMN-dependent monooxygenases have been determined, including C₂ of HPA hydroxylase, bacterial luciferase, SsuD and LadA. The structure of the C₂ enzyme, which differs significantly from the bacterial luciferase structural family, is a homotetrameric structure, with each monomeric structure consisting of an N-terminal, β -sheet, and C-terminal domain (Ellis, 2010). For the bacterial luciferase structural family, all members of this family form a TIM barrel structure, with the active site located at the C-terminal end of the β -barrel. LadA enzyme exists as a homodimer and SsuD a homotetramer. These two enzymes are more similar to each other when compared to the overall structure of the bacterial luciferase. Their monomeric units contain insertion regions that are not present in bacterial luciferase; moreover, they also have a C-terminal extension of the β -barrel structure (Eichhorn et al., 2002). For the flavin binding site, the first three-dimensional structure of FMN-dependent monooxygenase belongs to the C1 hydroxylase. The structure shows flavin binding in a pocket formed by the C-terminal and β -sheet domain, lined with a nonpolar region interacting with the dimethylbenzene region and a polar region which interacts with the pyrimidine portion of the ring (Alfieri et al., 2007). The reactions catalyzed by flavin-dependent monooxygenases varies from hydroxylation, Baeyer-Villiger oxidation, *N*-hydroxylation, epoxidation, to sulfoxidation (Pimviriyakul & Chaiyen, 2020a). For two-components system, the monooxygenase component is bound to the reduced flavin. During the reaction with oxygen, reactive intermediate such as C4a-(hydro)peroxyflavin (FL_{C4aOOH}, FL_{C4aOO}⁻) or N5-(hydro)peroxyflavin may formed. C4a-(hydro)peroxyflavin formation are usually found in phenolic hydroxylases responsible for the catalyzation of phenolic compound, the most extensively investigated two-component

hydroxylases are *p*-hydroxyphenylacetate-4-hydroxylase (C_2), which catalyze *p*-hydroxyphenylacetate hydroxylation (Sucharitakul et al., 2006). N5-(hydro)peroxyflavin was recently discovered as an intermediate of amide monooxygenase (RutA) catalyzing the oxidative amide cleavage in uracil catabolism (Adak & Begley, 2017). Later on, several enzymes such as EncM (Teufel et al., 2015), sulfone monooxygenase (DszA) (S. Adak & T. P. Begley, 2016), YxeK (Matthews et al., 2022) and flavin-dependent dehalogenases (HcbA1) (Adak & Begley, 2019) was found to generate N5-(hydro)peroxyflavin intermediate when reacted with oxygen. The difference between the two intermediates is that the enzyme active site promotes the substrate to bind near the O₂ and N5 position instead of the C4a of the isoalloxazine ring (Matthews et al., 2020).

1.3.2 The flavin dependent reductase

Structures of reductase components differ for each enzyme system. The three-dimensional structure of the FRP enzyme was shown to be a dimer of interlocking subunits, with each subunit comprised of two domains. In this structure, flavin was bound through hydrogen-bonding and hydrophobic interactions, providing evidence that the flavin is a tightly bound cofactor in FRP and cannot be transferred directly to its monooxygenase component (Tanner et al., 1996). The role of the reductase components in the family of FMN-dependent reductase enzymes is to catalyze the reduction of flavin and generate diffusible reduced flavin for the two-component flavin-dependent monooxygenases. Most reductases exist in homodimer form and are usually smaller than their monooxygenase counterparts. Reductase components differ from each other depending on their specificity for NADH, NADPH, and the ability to use either pyridine nucleotide. Furthermore, they are classified by whether the flavin cofactors are tightly bound and an external flavin is needed as a substrate in the catalysis, or the flavin cofactor is loosely bound and can be transferred to the monooxygenase component following the reduction by pyridine nucleotide (Ellis, 2010).

1.3.3 Flavin transfer mechanism

Once reduced flavin was generated, it dissociates from the reductase and bind to the monooxygenase due to different binding affinity and can occur without protein-protein interaction in some enzyme system (Sucharitakul et al., 2007; Sucharitakul et al., 2014). After the reaction is completed, the oxidized flavin dissociates from the monooxygenase component and returns to the reductase. The difference in affinity for a specific redox form of flavin help to ensure that the reduced flavin will be transferred and bound to the monooxygenase component for the catalyzation of the reaction (Ellis, 2010). The reduced flavin can also be re-oxidized by molecular oxygen found in the buffer instead of the oxygenase partner (Sucharitakul et al., 2014).

1.4 The use of co-immobilized enzymes for wastewater treatment

Research on the use of living systems such as microorganisms and plant to degrade pollutant in wastewater has been intensively studied. The use of biological systems for the degradation of the targeted pollutants was made possible due to their enzymes; therefore, these enzymes were explored as biochemical means of wastewater treatment (Ambatkar & Usha, 2012). The advantages of using enzyme include its high specificity to selected compounds, meaning that it can degrade targeted pollutants without affecting the other component in the system (Taylor et al., 1996). The enzymatic approach is favorable for the treatment of wastewater that contains relatively large amounts of the target pollutants. However, the use of free enzymes faces limitations related to enzyme stability and reusability since enzymes tend to denature outside their natural environment and are usually hard to isolate from the reaction system. To overcome these limitations, scientists had proposed the method of enzyme immobilization, a method that was used in industrial processes to minimize production costs from the uses of enzymes (Krajewska, 2004).

1.4.1 Co-immobilization of enzyme

Co-immobilization of the enzyme is usually required for uses on the industrial scale, since immobilization allows the enzyme to be reused and simplify the overall process, resulting in better cost efficiency and improved enzyme performance. This enhances in enzyme performance may

come from the support materials protecting enzyme from harsh environment and inhibition by other compounds. Moreover, immobilization of two-component enzymes helps to keep the monooxygenase and reductase components to be in close proximity, allowing better transfer of flavin (Cui et al., 2016; Mateo et al., 2007). Support materials used for the immobilization must be chosen depending on the type of enzyme to immobilize, immobilization techniques, and application of the co-immobilize enzyme. The ideal support materials must be inert, so it does not interfere with the reaction and should have a functional group on the surface with a high affinity to the targeted enzyme (Ren et al., 2019). Using magnetic nanoparticles as a support for enzyme immobilization can be beneficial due to their small size, large surface area, easily dispersed and the surface of the nanoparticles can be easily modified for reactive groups that have high affinity to the enzyme. Besides those characteristics, magnetic nanoparticles can be practically recycled using a magnetic field to separate them from the system (Zhang et al., 2011). One of the most common techniques used for immobilization of enzyme without loss of enzyme activity is based on using coordination between Ni^{2+} and histidine-tag on enzyme for high specificity and high affinity (de Almeida et al., 2018). This can be easily carried out by modifying the nanoparticle surface for immobilizing Ni^{2+} for affinity with histidine-tag of the target protein (Liao et al., 2020).



2. Methodology

2.1 Mechanism of two-component enzyme: Dimethyl sulphone monooxygenase

Reagents

Chromatographic media (G25 Sephadex, IMAC-Sepharose) were purchased from GE Healthcare (Uppsala, Sweden). FMN (purity $\geq 93\%$), NADH (purity $\geq 95\%$) and imidazole were purchased from Tokyo Chemical Industry (Tokyo, Japan). Guanidinium hydrochloride (GuHCl)

was purchased from Merck (Calbiochem) (Darmstadt, Germany). Concentrations of the following compounds were determined using their known extinction coefficients: NADH, $\epsilon_{340} = 6.3 \times 10^3 \text{ M}^{-1} \text{ cm}^{-1}$, FMN, $\epsilon_{445} = 12.5 \times 10^3 \text{ M}^{-1} \text{ cm}^{-1}$ at pH 7.0.

Native cofactor of the reductase component

The reductase component (DMSR) is a flavoprotein. The native flavin cofactor of the enzyme was characterized using 5% trichloroacetic acid (TCA) to separate the flavin from the precipitated enzyme. The unknown co-factor was analyzed using HPLC LC-20 Series (Shimazu, Japan) with a Shim-pack GIST C₁₈ column (4.6 × 250 mm) (Shimazu, Japan), and detected with a photodiode-array SPD-20A detector (Shimazu, Japan). The mobile phase (1 ml/min flow rate) for equilibration and separation was 1% formic acid (in H₂O) and 12% acetonitrile. The oven temperature was set to 25 °C. The flavin cofactor was determined based on the retention time of the flavin FAD and FMN standard compounds.

Determination of the molar absorption coefficients of the enzyme-bound FMN

The extinction coefficients of the flavin bound DMSR were determined using 2.68 M GuHCl. The released FMN concentration from the enzyme was calculated using the molar absorption coefficient for free FMN ($\epsilon_{445} = 12.5 \times 10^3 \text{ M}^{-1} \text{ cm}^{-1}$). The extinction coefficient of the FMN bound enzyme was calculated based on the released FMN concentration as $\epsilon_{448} = 11.0 \times 10^3 \text{ M}^{-1} \text{ cm}^{-1}$.

High yield expression of the monooxygenase component

The monooxygenase component of the DMSMO gene from *Acinetobacter baumannii* was synthesized by Genscript (USA), and subcloned into expression vector pET-22b containing a C-terminal His6-tag. The expression vector (ampicillin resistance) and the pTf16 chaperone plasmid (chloramphenicol resistance) for enhancing protein folding were co-transformed into competent *E. coli* ECOS™ Sonic (Yeastern Biotech, Taiwan). The transformed cells were selected on LB agar containing 20 µg/mL ampicillin and 20 µg/mL chloramphenicol. A transformed cell colony was inoculated in 50 ml starting media for auto-induction (in a 250 mL Erlenmeyer flask) containing

ampicillin and chloramphenicol as a starting culture for auto-induction. The starting culture was incubated at 37 °C overnight in an incubator shaker (Unimax 1010 & Incubator 1000) (Heidolph, Germany).

The overnight culture was inoculated into 1 L of auto-induction media in a 2.5 L Fernbach flask. A sterile L-arabinose (0.5 mg/ml) solution was added to the large-scale culture for inducing chaperone expression. The large-scale culture was incubated in a multitron incubator with an orbital shaker (INFORS HT Multitron, Switzerland) at 37 °C for ~3 h or the optical density at 600 nm was ~1. The temperature of the incubator was decreased to 20 °C. The large-scale culture was left overnight (~18 h). The cells were harvested and kept at -80 °C.

The frozen cell pellet was thawed in lysis buffer (50 mM potassium phosphate, pH 7.0 containing 50 mM imidazole and 300 mM NaCl). The cells were lysed using an ultrasonic sonicator VCX750 (Sonics & Materials, USA) with an energy of 75 Amps, 6 sec pulse on and 10 sec pulse off. The sample was kept cool in an ice bath during sonication. The resulting cell debris suspension was centrifuged by an Allegra™ 64R Centrifuge (Beckman Coulter, USA) at 18,000 rpm for 1 h at 4 °C to collect the supernatant.

The supernatant was loaded onto an IMAC Sepharose™ (GE Healthcare, USA) (2.5 ϕ × 12 cm) column charged with 100 ml 0.2 M nickel sulfate solution. The column was pre-equilibrated with 200 ml 50 mM sodium phosphate pH 7.0 containing 300 mM NaCl and 50 mM imidazole. After loading the sample, the column was washed with 500 ml of the same buffer. High expression of the monooxygenase component demonstrated that some of the enzyme bound with FMN. The FMN bound on the enzyme was removed by washing the column with 500 mL 50 mM sodium phosphate pH 7.0 containing 1 M KBr, 25 mM imidazole and 300 mM NaCl. The enzyme was eluted with 50 mM sodium phosphate (pH 7.0) containing 300 mM NaCl and 200 mM imidazole. The purification procedure was performed at 4 °C. Fractions containing DMSO were identified by sodium dodecyl sulfate-polyacrylamide gel electrophoresis (SDS-PAGE). The enzyme fractions were concentrated by ultrafiltration using an Amicon® cell-stirring device (Merck, Germany) with

a molecular mass cutoff of 10 kDa to decrease the solution volume to ~ 5 mL. The concentrated enzyme was passed through a desalting column Sephadex G-25 ($1.5 \phi \times 45$ cm) to remove salts and imidazole.

High yield expression of the reductase component

The reductase component gene from *Acinetobacter baumannii* was synthesized by Genscript (USA), and subcloned into expression vector pET-22b containing a C-terminal His6-tag. The expression vector (ampicillin resistance) was transferred into competent *E. coli* ECOSTM Sonic (Yeastern Biotech, Taiwan). The transformed cells were selected on LB agar containing 20 μ g/ml ampicillin. A transformed cell colony was inoculated in 50 ml starting media for auto-induction (in a 250 mL Erlenmeyer flask) containing ampicillin as a starting culture for auto-induction. The starting culture was incubated at 37 °C overnight in an incubator shaker (Unimax 1010 & Incubator 1000) (Heidolph, Germany).

The overnight culture was inoculated into 1 L of auto-induction media in a 2.5 L Fernbach flask. The large-scale culture was incubated in a multitron incubator with an orbital shaker (INFORS HT Multitron, Switzerland) at 37 °C for ~ 3 h or optical density at 600 nm was ~ 1 . The incubator temperature was reduced to 25 °C. The large-scale culture was left overnight (~ 18 hours). The cells were harvested and kept at -80 °C.

The frozen cell pellet was thawed in lysis buffer (50 mM potassium phosphate, pH 7.0 containing 100 mM imidazole and 300 mM NaCl). The cells were lysed using an ultrasonic sonicator VCX750 (Sonics & Materials, USA) with an energy of 75 Amps, 6 sec pulse on and 10 sec pulse off. The sample was kept cool in an ice bath during sonication. The resulting cell debris suspension was centrifuged by an AllegraTM 64R Centrifuge (Beckman Coulter, USA) at 18,000 rpm for 1 h at 4 °C to collect the supernatant.

The supernatant was loaded onto an IMAC SepharoseTM column pre-equilibrated with 50 mM potassium phosphate pH 7.0, 100 mM imidazole, and 300 mM NaCl. The column was washed with 500 ml of the same buffer. The purification procedures were performed at 4 °C. The intense

yellow band containing the enzyme-bound flavin was detected on the top of the column. The intense yellow color fraction was eluted with 300 mM imidazole in the same buffer. FMN was supplemented for flavin cofactor saturation during the concentrating process using an Amicon® cell-stirring device (Merck, Germany) with a molecular weight cutoff of 10 kDa. The purified enzyme was passed through a desalting column Sephadex G-25 gel filtration column (1.5 ϕ \times 45 cm) to remove excess FMN and salts.

Determination of the native molecular weights of the reductase and monooxygenase components

The purified reductase and monooxygenase were loaded into a 2.5 ϕ \times 71.5 cm Sephacryl S-200 gel-filtration column. The column was attached to a fast protein liquid chromatography (FPLC) machine (ÄKTA pure 25 M1, Cytiva, US). The column was equilibrated with 50 mM potassium phosphate containing 300 mM NaCl, pH 7.0 with a flow rate of 0.5 ml/min and eluted with the same buffer at room temperature. The eluents were monitored at 280 and 458 nm using a UV-absorption detector. The molecular weight was determined using a standard calibration curve obtained from a Gel filtration Calibration Kit HMW (Ovalbumin: 43 kDa, Conalbumin: 75 kDa, Aldolase: 158 kDa, Ferritin: 440 kDa, Blue Dextran 2000: > 2000 kDa). The void volume of the column was determined from the blue dextran elution volume.

Thermodynamic binding of the oxygenase component to oxidized FMN

Free FMN was titrated with the purified oxygenase component. The reaction was performed in 50 mM potassium phosphate pH 7.0 at 25 °C. The FMN bound enzyme fraction was determined from the decrease in the fluorescent signal of FMN observed using a spectrofluorometer RF5301PC (Shimadzu, Japan). To determine the dissociation constant (K_d), the intensity change of the emission peak at 445 nm (ΔF) was plotted *versus* free enzyme concentration. The K_d for the enzyme binding to FMN was obtained from a plot using the following equation (Equation 1):

$$\Delta F = \frac{[E_T] + K_d - \sqrt{([E_T] + [S_T] + K_d)^2 - 4[E_T][S_T]}}{2[FMN]_{total}} \times \Delta F_{max}$$

Equation 1. General quadratic equation based on having no assumption for steady-state equilibrium binding

Rapid kinetic studies

The rapid kinetic studies were performed using stopped-flow spectrophotometry Model SF-61DX (TgK Scientific, UK) in single-mixing mode. The absorbance was detected using a charge-coupled device (CCD) and photomultiplier tube. The emission intensity was detected using a photomultiplier tube coupled with optical filters. The stopped-flow measurements were performed in 50 mM potassium phosphate buffer, pH 7.0, 25 °C. The concentrations described were after mixing.

Oxygen scrubbing the flow system in stopped-flow spectrophotometer

To obtain anaerobic conditions, the stopped-flow apparatus was equilibrated and flushed with sodium hydrosulfite (~5 mg/mL) in 100 mM potassium phosphate pH 7.0, which was prepared in a closed system tonometer under positive nitrogen (ultrahigh pure, 99.999%). The buffer was alternatively equilibrated and evacuated for forty cycles. The last cycle was under positive nitrogen pressure (~4 Psi) in a closed container tonometer, and then sodium dithionite powder in the side arm attached to the tonometer was flipped into the anaerobic solution. The anaerobic sodium dithionite solution in the tonometer was transferred into the flow system of the stopped-flow instrument equilibration overnight (~16 h). Before the experiment was performed, the flow system was washed three times with anaerobic buffer.

The kinetic mechanism for binding of FMN-DMSMO complex with DMSO₂

The kinetic binding of FMN:DMSMO complex with DMSO₂ was performed by mixing a solution of FMN:DMSMO complex with varied concentrations of DMSO₂. The binding of DMSO₂ to FMN:DMSMO complex was monitored by the fluorescence quenching of FMN bound DMSMO. The observed rates were analyzed by the decrease in fluorescence intensity obtained from the kinetic traces. A plot of observed rate constants (k_{obs}) versus DMSO₂ showed hyperbolically dependent indicating the mechanism of a two-step equilibrium: the first rapid equilibrium binding of FMN:DMSMO complex with DMSO₂ to form Michaelis-Menten complex following the isomerization according to Equation 2. The significant intercept indicated an

existence of the reversible rate (k_{-3}). According to Equation 2, K_d was identified from the concentration of the half-saturation of hyperbolic plot, whereas k_3 was from the limit to infinity value of the rate constants (or maximum value). $[S]$ represented the concentrations of DMSO_2 under pseudo-first order condition.

$$k_{obs} = \frac{k_3[S]}{K_d + [S]} + k_{-3}$$

Equation 2. Equation derived from the simulation model (**Figure 5**) to calculate k_{obs} from experimental data

Rapid kinetics of the oxygenase component (DMSMO)

The rapid kinetic study of the oxidative reactions were performed using either free reduced FMN or reduced FMN:DMSMO complex reacting with oxygenated buffer. The free FMN or its complex with monooxygenase solution was made anaerobic in the tonometer using the same procedure as described above. A 5 mg/ml dithionite solution (reductant) was made anaerobic by bubbling it with nitrogen gas from a long needle in a glass syringe for 6 min. A micro-titrator with a long needle was filled with anaerobic dithionite solution, and the micro-titrator was attached to the tonometer via a Michael-Miller adaptor under positive nitrogen pressure. The dithionite solution was put into the solution in the tonometer by turning the knob of the micro-titrator. The stoichiometric reduction of the solution was monitored by flipping the solution into the side arm attached with a quartz cuvette to observe the changing spectra of the oxidized to fully reduced flavin without excess dithionite. The spectral change from flavin reduction was monitored using a spectrophotometer with a diode array detector (Cary 8454 UV-Vis, Agilent Technologies).

The buffers with different oxygen concentrations were prepared by bubbling 6 ml of the buffer with a mixture of nitrogen and oxygen, i.e., 20%, 50% and 100%, (before mixing) for 6 min in a glass syringe. After equilibration, the syringe containing the oxygenated buffer was transferred to a stopped-flow machine, and the oxygen concentration after mixing was 0.13, 0.31, 0.61, and 0.96 mM, respectively.

Rapid kinetics reduction of the reductase component (DMSR)

The kinetic reduction of DMSR was performed by mixing anaerobic solution of the oxidized enzyme with anaerobic solution of NADH with varied concentrations with the lowest concentration being at least 5-fold higher than the oxidized enzyme. The oxidized enzyme was prepared in a tonometer using anaerobic train for evacuation and equilibration of UHP nitrogen gas as described above. The anaerobic enzyme solution was transferred from a tonometer to the drive syringe of the stopped-flow machine. The varied NADH concentrations were made anaerobic by bubbling with UHP nitrogen gas via long needle syringe and then transferred to the drive syringe. Both enzyme and NADH were mixed in the stopped-flow machine. The reactions were monitored using absorbance in range of 350 – 700 nm for flavin semiquinone, flavin reduction and charge-transfer complex.

Kinetic analysis and simulations

The absorbance or fluorescence kinetic traces were analyzed using Kinetic Studio software (Hi-Tech Scientific, UK) to obtain the observed rate constants. The models fitted for rate constant analysis were initiated with the simplest one-exponential phase before being extended to more complex models.

The bimolecular reactions of enzyme with substrates were performed under pseudo-first order conditions using substrate concentrations at least 5-fold excess over the enzyme concentration to obtain the observed rate constants (k_{obs}). The reaction mechanisms were analyzed from plots of the observed rate constants *versus* various substrate concentrations. The relationship of the observed rate constants and the individual rate constant according to the reaction mechanism was analyzed using Marquardt–Levenberg nonlinear fit algorithms included in KaleidaGraph (Synergy Software 4.5).

In case of complex reaction mechanisms, kinetic simulation was performed to verify the mechanism models using the enzyme kinetic software Kintek Explorer 9. The kinetic traces obtained from the simulations were overlaid with the experimental traces to confirm the proposed mechanism model.

Free reduced FMN released from reduced DMSR

The percentage of free reduced FMN released from reduced DMSR was determined using sephadex G-10gel filtration. The column was equilibrated with 50 mM potassium phosphate pH 7.0 containing 5 mM sodium bisulfite. The 2.5 ml 400 μM DMSR solution was loaded into the column. The oxidized bright yellow DMSR was reduced in a buffer containing sodium bisulfite and became colorless. The reduced enzyme was collected with 3.5 ml of the column void volume. One ml fractions were collected up to 22 ml. The fractions were left for 30 min to be fully oxidized. The fully oxidized enzyme and free FMN were confirmed by scanning the spectra until no change was observed. The fractions containing free FMN were pooled and the total volume was measured. The pooled FMN concentration was determined from its absorption spectrum. The amount of free FMN was calculated to obtain the concentration of free FMN released in the reduced 400 μM DMSR solution.

Product identification from single turnover reactions

A 300 μM DMSMO and 56 μM FMN in 50 mM potassium phosphate pH 7.0 solution was made anaerobic in a close system tonometer under positive nitrogen pressure. The enzyme solution was reduced by freshly prepared sodium dithionite. The anaerobic procedures and enzyme reduction were described in the previous section on the rapid kinetic studies. The reduced enzyme solution was mixed with an equal volume of air-saturated buffer containing 5 mM DMSO_2 at room temperature. The enzyme and small molecules in the reaction were separated using ultrafiltration with 10 K Amicon[®] Ultra filters (Merck, Ireland). The methanesulfinate product was analyzed using a 1260 Infinity HPLC (Agilent Technologies, USA) with a 4.6 ϕ \times 250 mm Shim-pack GIST C18 column (Shimazu, Japan). The column was equilibrated with a mobile phase of 10% acetonitrile and 5% formic acid in H_2O with a flow rate of 0.5 ml/min. The methanesulfinate was detected with a Quadrupole LC/MS 6120 mass detector (Agilent Technologies, USA), set to detect an m/z of 79 (negative mode). The total retention time of the analysis was 10 min.

Analysis of the hydroxylation reaction using rapid-quench flow techniques

The experiments were performed using rapid-quench flow (model: RQF-63) from TgK Scientific (Bradford-on-Avon, UK) in an anaerobic glove box. The rapid-quench flow system consisted of three syringes: Syringe A contained an anaerobic solution of 112 μM reduced Reductase mixed with 600 μM reduced monooxygenase enzyme. Syringe B contained a 0.15 M HCl quencher solution. Syringe C contained an air-saturated buffer (0.26 mM oxygen) with 10 mM dimethylsulfone. The reduced enzyme complex solution was mixed with the air-saturated buffer and the reaction mixture was allowed to age for 0.01, 0.02, 0.04, 0.05, 0.06, 0.07, 0.08, 0.1, 0.2, 0.4, 0.6, 0.8, and 1 sec, before being quenched with a 0.15 M HCl solution. The quenched samples were collected from the sample loop, and the enzyme was separated using ultrafiltration with 10 K Amicon[®] Ultra filters (Merck, Ireland). The samples were analyzed for the amount of methanesulfinate produced from the reaction using a 1260 Infinity HPLC (Agilent Technologies, USA) with a 4.6 ϕ \times 250 mm Shim-pack GIST C18 column (Shimadzu, Japan). The column was equilibrated with a mobile phase of 10% acetonitrile and 5% formic acid in H₂O with a flow rate of 0.5 ml/min. The methanesulfinate product was detected with a Quadrupole LC/MS 6120 mass detector (Agilent Technologies, USA), set to detect an m/z of 79 (negative mode). The total retention time of the analysis was 10 min.

The concentrations of methanesulfinate from the rapid-quenched flow were determined from a calibration curve of the area under the mass peaks *versus* 10 μM , 25 μM , 50 μM , 75 μM and 100 μM methanesulfinate standards. Each methanesulfinate standard concentration was prepared by mixing with an equal volume of 0.15 M HCl before being injected into the LC-MS machine. The observed rate constant (k_{obs}) was determined from a plot of methanesulfinate concentrations *versus* quenched times as described above. The observed rate constant was analyzed from Equation 3 using Marquardt–Levenberg nonlinear fit algorithms included in KaleidaGraph (Synergy Software 4.5). P and P_{∞} is the product forming at any time and is the limited value of the product close to infinity of time.

$$P = P_{\infty}(1 - e^{-k_{\text{obs}}t})$$

Equation 3. Equation derived from Marquardt–Levenberg nonlinear fit algorithms for k_{obs}

Formaldehyde identification and quantification

Formaldehyde was identified using purpald reagent (4-amino-3-hydrazino-5-mecapto-1,2,4-triazole). 0.5 M purpald solution in 2 M NaOH was added to a 1 mL assay reaction at a final concentration of 34 mM. The assay reaction was incubated for 10 mins at room temperature prior to oxidize by adding 0.18 M H_2O_2 . The absorbance was measured at 512 nm. The concentrations of formaldehyde in the assay reaction were determined using a calibration curve of 10, 20, 40, 60, 80, and 100 μM formaldehyde.

Formaldehyde was identified using multiple- and single-turnover reactions. The enzyme multiple turnover reactions were composed of 56 μM DMSR, 300 μM DMSMO, 1 mM NADH and 5 mM DMSO_2 . The reaction was started by adding NADH and left at room temperature for 30 min. The solution containing the formaldehyde product was separated by Amicon ultra centrifugal filters (10 kDa cut off). To quantify the formaldehyde product from the single-turnover reaction, a 56 μM DMSR and 300 μM DMSMO solution was put in a tonometer that had a connector attached to a three-way oblique manifold for vacuum and evacuation of positive nitrogen (ultrahigh pure, 99.999%). The microtitrator attached to a gastight syringe with a long needle containing anaerobic NADH solution was connected to the tonometer by a Michel-Miller adapter. The stoichiometric reduction of the enzyme solution was performed as described in the Rapid kinetic studies section. After complete reduction, the tonometer was opened and an equal volume of air-saturated buffer was added to re-oxidize the enzyme. The proteins in the solution were separated using ultrafiltration and the formaldehyde product in the filtrate was quantitated.

H_2O_2 identification

H_2O_2 was identified using 2,2'-azino-bis (3-ethylbenzthiazoline-6-sulphonic acid) (ABTS) and horseradish peroxidase (HRP). Single turnover reactions were performed in three conditions: 1) 56 μM DMSR, 2) 56 μM DMSR and 300 μM DMSMO and 3) 56 μM DMSR, 300 μM DMSMO and 5 mM DMSO_2 . After mixing with the air-saturated buffer, 1 mM ABTS and 5 units HRP was

added to the solution. The H_2O_2 concentration was determined by the concentration of oxidized ABTS in a 1:1 ratio, the absorbance was measured at 735 nm with an extinction coefficient of $\epsilon_{735} = 9.32 \times 10^3 \text{ M}^{-1} \text{ cm}^{-1}$.

2.2 Co-immobilization of enzymes onto CoFe_2O_4 magnetic nanoparticle

Reagents

All chemicals were used as purchased without further purification. Iron(III) nitrate (FeN_3O_4 , 98%), cobalt chloride ($\text{Co}(\text{NO}_3)_2$, 98%), ethylene glycol (anhydrous, 99.8%), ammonium acetate ($\text{CH}_3\text{CO}_2\text{NH}_4$, $\geq 97\%$), 3-aminopropyltriethoxysilane (APTES, $\geq 98\%$), hexane (AR grade), Glutaraldehyde (25% Aqueous solution), $\text{N}\alpha,\text{N}\alpha$ -Bis(carboxymethyl)-L-lysine hydrate (ANTA, $\geq 97.0\%$), sodium borohydride (NaBH_4 , $\geq 98.0\%$), Nickel(II) sulfate hexahydrate ($\text{NiSO}_4 \cdot 6\text{H}_2\text{O}$, $\geq 98.0\%$) were purchased from Sigma-Aldrich (MO, USA).

Synthesis of CoFe_2O_4 and $\text{Ni-NTA}/\text{H}_2\text{N-SiO}_2@/\text{CoFe}_2\text{O}_4$

4 mmol FeN_3O_4 and 2 mmol $\text{Co}(\text{NO}_3)_2$ were dissolved in 50 mL ethylene glycol under vigorous stirring (600 rpm, 20 min) before adding 30 mmol ammonium acetate under ultrasonic for 30 min to form clear dark yellow solution. The solution was vigorously stirred (600 rpm) for another 30 min at RT before transferred to 100 mL Teflon-line autoclave, fixed and kept in at 210°C , 24 h. Once cooled down, the black precipitate was collected using a magnet and rinsed several times with DI water and ethanol before dried in a 50°C oven. $\text{H}_2\text{N-SiO}_2@/\text{CoFe}_2\text{O}_4$ was obtained by dispersing CoFe_2O_4 in Hexane for 10 min before 200 μL APTES was added, the solution was ultrasonic for 1 h before rinsed with ethanol and dried. To obtain $\text{Ni-NTA}/\text{H}_2\text{N-SiO}_2@/\text{CoFe}_2\text{O}_4$, the particles was stirred in 10% glutaraldehyde solution for 8 h at RT. The solution was washed with DI water and dispersed in 10 mL Tris-HCl buffer (50mM, pH8.0). 48 mg of ANTA was added to the solution and stirred at RT for 8 h before 10 mg NaBH_4 was added and stirred for another 1 h. After completion, the mixture was washed several times with Tris-HCl and suspended in 5mL of 2M NiSO_4 solution and stirred for 2 h. $\text{Ni-NTA}/\text{H}_2\text{N-SiO}_2@/\text{CoFe}_2\text{O}_4$ was collected using a magnet and washed with DI water before dried in 50°C oven.

Characterization of Ni-NTA/H₂N-SiO₂@CoFe₂O₄

The morphologies and nanocomposites of the synthesized Ni-NTA/H₂N-SiO₂@CoFe₂O₄ were characterized by scanning electron microscopy (SEM) coupled with energy-dispersive X-ray spectroscopy (EDX: JEOL JSM-6610LV, Oxford X-Max 50). CoFe₂O₄ magnetic nanoparticle character was verified using an X-ray powder diffractometer (DMAX2200/Ultima-plus instrument, Rigaku, Japan).

Immobilization of His-tagged DMSMO and DMSR onto Ni-NTA/H₂N-SiO₂@CoFe₂O₄

His-tagged DMSMO and DMSR were mixed in a ratio of 5:1 before added to Ni-NTA/H₂N-SiO₂@CoFe₂O₄ particles dispersed in phosphate buffer (50mM, pH7.0). The mixture was swirled on an orbital shaker (IKA KS 260, China) at 150 rpm, on ice, for 1 h. Immobilized enzymes were collected using a magnet and washed with phosphate buffer several times. To study the specificity of Ni-NTA functionalized nanoparticles to His-tagged enzymes, imidazole solution (300 mM, pH7.0) was used to elute the enzyme from the surface of the nanoparticles. The eluted enzyme was analyzed by sodium dodecyl sulfate polyacrylamide gel electrophoresis (SDS-PAGE).

DMSMO activity assay

DMSMO activity assay was carried out by mixing DMSMO, DMSR, NADH and DMSO₂ for a multiple turnover reaction at room temperature. After the reaction was completed, 34 mM Purpald, dissolved in 1 M NaOH, and 0.18 M H₂O₂ was added to the reaction mixture. The mixture was vigorously shaken and left at room temperature for 1h before the absorbance was measured at 505 nm. The concentrations of formaldehyde in the assay reaction were determined using a calibration curve of 10, 20, 40, 60, 80, and 100 μM formaldehyde.

Stability and reusability test

To determine the storage stability, free DMSMO mixed with DMSR and co-immobilized DMSMO-DMSR, stored at 4°C, was used for activity assay after being stored for 1, 2, 4, 6, 8 and 10 days. The enzyme activity of Day 1 was taken as 100%. For temperature stability, DMSMO and

DMSR were mixed together and left to incubate at 4, 20, 30, 40, 50°C prior to the reaction. The highest activity was set as 100% for reference. pH stability was determined by performing multiple turnover reaction in 50 mM phosphate buffer with pH range of 2-10 at room temperature. The highest activity at pH7 was set as 100% for reference. The reusability of co-immobilized DMSMO-DMSR was performed at room temperature. The co-immobilized DMSMO-DMSR were recovered from the solution using a magnet after each reaction, rinsed with 50 mM phosphate buffer (pH7.0) and stored at 4°C.

3. Results

3.1. Mechanistic study of enzymes

3.1.1 Enzyme characterization

The monooxygenase component (DMSMO) and reductase component (DMSR) recombinant C-terminal histidine-tagged enzymes were successfully expressed as soluble enzymes in *E. coli*. After purification, the pure protein yield was approximately 21 g/l of cell culture for DMSMO and 3 g/l of cell culture for DMSR. The purity of both proteins was > 95% as determined by SDS-PAGE (**Figure 1**).

The FPLC equipped with size-exclusion chromatography to determine the native molecular weight of DMSMO and DMSR revealed a molecular mass of 92.3 kDa and 136.6 kDa, respectively. The molecular weight calculation of the DMSMO and DMSR subunit using amino acid sequences was 41.8 kDa and 26.6 kDa, respectively. The results suggested that the native form of DMSMO and DMSR was a dimer and tetramer, respectively.

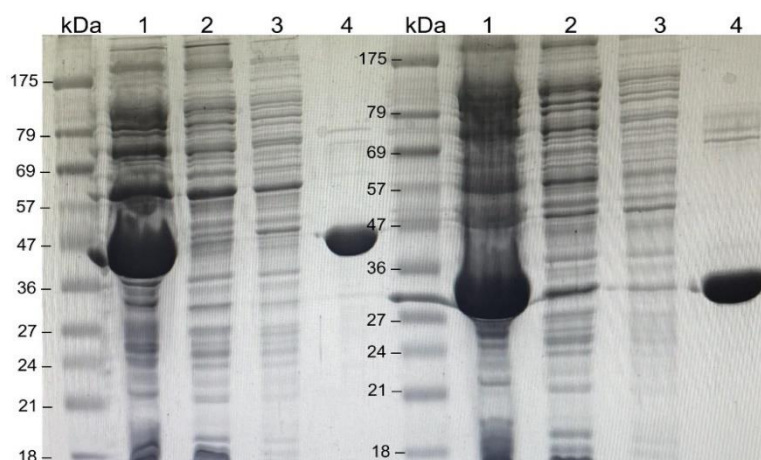


Figure 1. SDS-PAGE (12%) of DMSR and DMSMO. High-yield expression of both components of the DMSMO and the DMSR. Both components were purified using affinity chromatography IMAC sepharose. Left panel: purification of DMSMO. Right panel: purification of DMSR. Lane: molecular weight markers, Lane 1: crude extract, Lane 2: flow-through fraction, Lane 3: washing fraction, Lane 4: elution fraction.

The purified DMSMO solution had a slightly yellow color with characteristics of an enzyme bound to oxidized flavin (**Figure 2A and 2B**). To determine the native flavin bound enzyme, the flavin was separated from the enzyme using 5% trichloroacetic acid. FAD and FMN flavins standards were used to identify the native flavin from the denatured proteins. The isolated flavin cofactor from DMSMO had a peak at retention time of 11.5 min (black line, **Figure 2C**), which was the FMN retention time (red line, **Figure 2C**). The isolated flavin cofactor from DMSR had a peak at retention time of 9.82 min (black line, **Figure 2D**), which was the retention time of FMN (red line, **Figure 2D**). The purified DMSMO and DMSR were bound with FMN. The flavin content of DMSMO was determined using 5% TCA. The released free flavin was calculated to be 37.1%.

The product of the catalytic reaction was analyzed using LC-MS that detected a methanesulfinate mass of 79 m/z. However, there were two peaks with the same mass at a retention time of 5.32 and 6.3 min when the methanesulfinate standard (dissolved in potassium phosphate)

was injected (**Figure 2E**). The peak with a retention time of 5.32 min was confirmed as the buffer content of phosphite anion when only 50 mM potassium phosphate was injected into the LC-MS at the same conditions used for analyzing methanesulfinate (**Figure 2F**). The catalytic reaction of the enzymes was investigated using the methanesulfinate generated from the multiple turnover reaction in the presence of DMSR, DMSMO, NADH, DMSO₂ and atmospheric oxygen. Phosphite anion and methanesulfinate peaks were observed (**Figure 2G**).



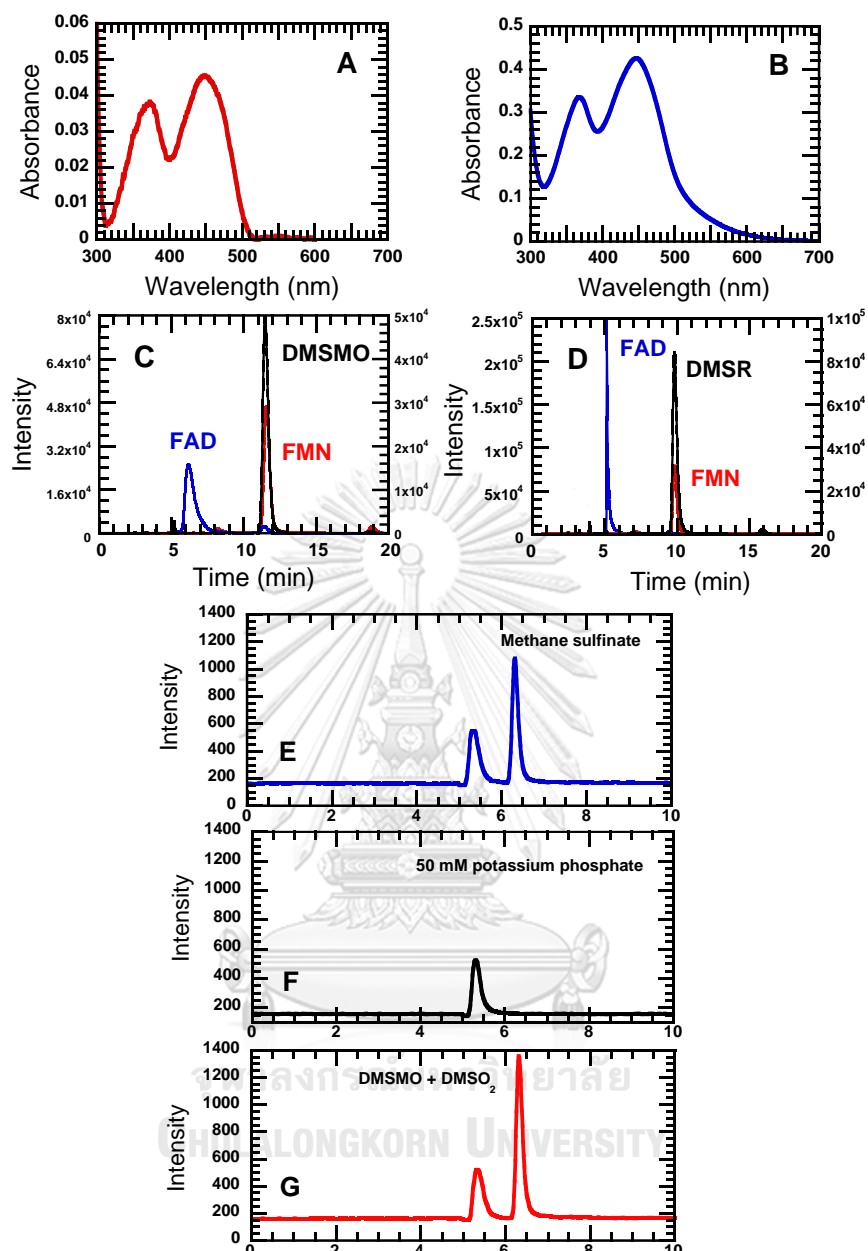


Figure 2. Native cofactor and product characterization of the DMSMO system (A) Spectrum of flavin bound DMSMO (red line). (B) Spectrum of flavin bound DMSR (blue line). Both enzymes were denatured using 5% trichloroacetic acid to release the native flavin cofactor. The cofactor was identified using HPLC. (C) HPLC chromatogram representing the separation of FAD (blue line) standard and FMN (red line). Black lines are the chromatograms of the isolated native flavin from DMSMO (D) HPLC chromatogram representing the separation of the FAD (blue line) standard and FMN (red line). Black lines are the chromatograms of the isolated native flavin from DMSR (E) Methanesulfinate (product of DMSMO) standard in 50 mM potassium phosphate pH 7.0 was detected using LC-MS equipped with C_{18} column. (F) 50 mM potassium phosphate pH 7.0. (G) 5 μ l of the enzyme multiple turnover reaction. The reaction contained 1 mM NADH, 5 mM $DMSO_2$ and 56 μ M DMSR, and 300 μ M DMSMO.

To demonstrate that formaldehyde is another product from a one-carbon cleavage from dimethyl sulfone, purpald reagent was used to detect formaldehyde from the multiple and single turnover reactions (see **Methods**). For multiple turnover reaction, 96 μM formaldehyde (9.6% based on 1 mM NADH as limiting agent) was detected. 19 μM formaldehyde (34% based on 56 μM reduced DMSR) was calculated from single turnover reaction.

3.1.2 Binding of DMSMO to oxidized FMN

The static binding of DMSMO to oxidized FMN was performed by titrating free FMN with various enzyme concentrations. The binding of enzyme to FMN resulted in quenched fluorescence intensity (**Figure 3A**). The dotted red-line spectrum represents free FMN and the solid lines represent a decrease in emission intensity after being titrated with DMSMO. The dotted line was used as a reference for the difference in the intensity change after titration. The difference in intensity at 528 nm from protein binding to FMN was used to calculate the FMN-bound enzyme concentrations. The dissociation constant (K_d) of the complex was determined from a plot of [ES] versus enzyme concentrations (**inset Figure 3A**). The K_d of $17.4 \pm 0.9 \mu\text{M}$ was calculated from a curve fit of the plot using Equation 1.

The rapid kinetic binding of DMSMO to oxidized FMN was performed by mixing 5 μM FMN with various enzyme concentrations under a pseudo-first order condition ($[\text{DMSMO}] \gg \text{FMN}$ at least 5-fold). The binding of DMSMO to oxidized FMN demonstrated a rapid decrease in fluorescence intensity ($\geq 530 \text{ nm}$) (**Figure 3B**). The enzyme bound to FMN very fast, and partially occurred during the dead time (before 1 ms). At the highest concentration of DMSMO (320 μM), most of the fluorescence intensity change was in the dead time (the lowest black line, **Figure 3B**). Therefore, a kinetic simulation was required for constructing the reaction mechanism. The simplest model of a single-step binding enzyme to oxidized FMN was applied as seen in the red-dotted lines (**Figure 3B**). The simulation kinetic traces were almost superimposed with the experimental data (black lines in **Figure 3B**). The bimolecular rate constant from the simulation for enzyme binding to oxidized FMN was $4.21 \times 10^6 \text{ M}^{-1} \text{ s}^{-1}$ (k_f , Table 1) with a reverse rate constant of 92.3 s^{-1} (k_r ,

Table 1). The K_d (k_f/k_r) from the forward and reverse rate constant was calculated to be 22 μM , which was similar to the K_d from static titration (17 μM). This confirmed that the binding mechanism of DMSMO to oxidized FMN is a single-step process.

3.1.3 Binding order of FMN and DMSO₂ to DMSMO to form a ternary complex

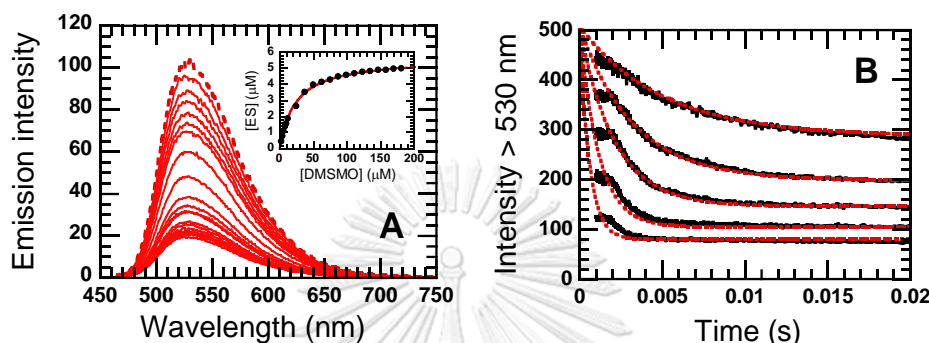


Figure 3. Static and kinetic binding of DMSMO to FMN. (A) 5 μM FMN solution was titrated with various concentrations of DMSMO. The binding of enzyme to FMN was monitored via fluorescence quenching. The reaction was performed in 50 mM potassium phosphate pH 7.0 at 25 $^{\circ}\text{C}$. The dotted line represented the emission spectrum of free FMN. The solid lines showed the quenched emission spectra according to the higher enzyme concentrations. Inset (A) is the plot of [ES] complex versus DMSMO concentrations. (B) 5 μM FMN solution was mixed with 20 μM , 40 μM , 80 μM , 160 μM , 320 μM DMSMO in a stopped-flow spectrometer. The kinetic binding was monitored based on a decrease in fluorescence intensity (cut off optical filter ≥ 530 nm). The reactions were performed in the same condition as previously described in (A). The black lines are the kinetic traces from the experimental data. The red dotted lines are from the simulation using a single-step binding model.

The previous results revealed that DMSMO bound to oxidized FMN (**Figure 3**). We next investigated the binding order of FMN and DMSMO when a substrate is present. A 5 μM free FMN solution was mixed with 20 μM DMSMO and 5 mM DMSO₂. The reaction was monitored based on a decrease in emission intensity using an optical filter (≥ 530 nm cut off). The kinetic traces with a decreased emission intensity indicated two exponential phases (green line, **Figure 4A**). The first exponential phase (1 ms–0.2 s) of the green line was superimposed with the red line,

which was the trace from mixing of FMN with DMSMO, indicating that the first exponential phase of the green line was DMSMO binding to FMN. The second exponential phase (0.2–1 s) of the green line continuing from the first exponential phase was present only in the presence of DMSO₂ (**Figure 4A**). These results demonstrated that in the presence of FMN, DMSMO and DMSO₂, FMN binds to DMSMO first, followed by DMSO₂. The control reactions from mixing 5 μM FMN with buffer and with 5 mM DMSO₂ are seen in the blue and black line, respectively. Neither mixing experiment contributed to the intensity change.



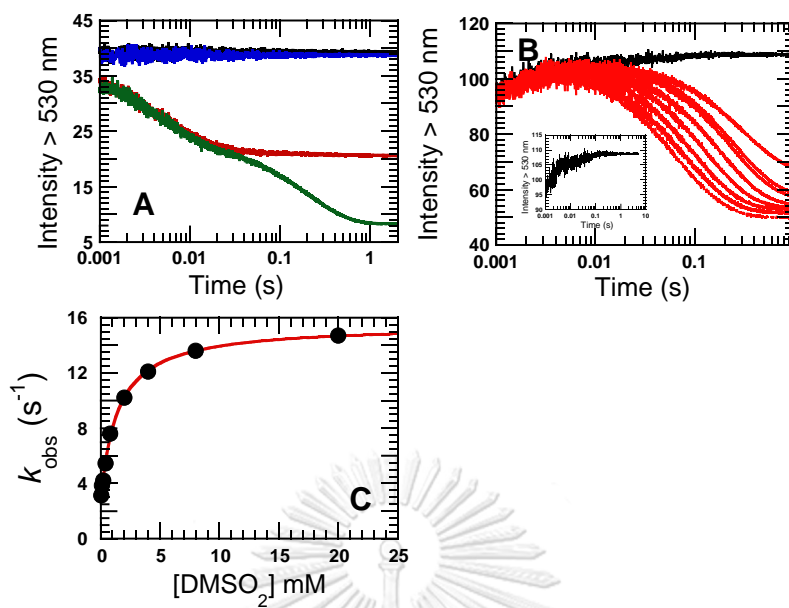


Figure 4. Mechanism of DMSMO binding to DMSO₂ and FMN. (A) Red line: 5 μM FMN solution mixed with 20 μM DMSMO. Green line: 5 μM FMN solution mixed with pre-equilibrated 20 μM DMSMO and 5 mM DMSO₂ solution. Blue and black lines are control reactions: 5 μM FMN solution was mixed with buffer and 5 mM DMSO₂, respectively. (B) Pre-equilibrated 15 μM FMN and 150 μM DMSMO was mixed with 0.05, 0.1, 0.2, 0.4, 0.8, 2, 4, 8, 20 mM DMSO₂. The uppermost trace was control from mixing FMN:DMSMO complex with buffer. The kinetic trace is magnified in **inset B**. The most right to the most left traces were from the lowest DMSO₂ concentration to the higher concentrations. (C) The observed rate constants (k_{obs}) analyzed from the kinetic traces in (B) were plotted against DMSO₂ concentrations.

Reaction was performed in 50 mM potassium phosphate pH 7.0 at 25 °C using stopped-flow spectrophotometer. All concentrations as described were after mixing. The reactions were monitored using fluorescence intensity change with optical filter ≥ 530 nm.

The mechanism of DMSO₂ binding to the FMN:DMSMO complex was elucidated by mixing pre-equilibrated 150 μM DMSMO and 15 μM FMN with various DMSO₂ concentrations. The binding was monitored using a decrease in fluorescence intensity change greater than 530 nm. The various DMSO₂ concentrations kinetic traces demonstrated three exponential phases. The first exponential phase (1–5 ms) was a slight increase in the emission intensity. This phase was independent of DMSO₂ concentration. The control reaction of mixing pre-equilibrated DMSMO

and FMN with buffer (without DMSO₂) (black line in inset of **Figure 4B**) had an exponential phase where some of the FMNH⁻:DMSMO complex dissociated to free FMN and free enzyme, resulting in an increase in fluorescence intensity, which was the reverse reaction to **Figure 3B** (k_1 and k_{-1} , **Figure 5**). This exponential phase was also found in the various DMSO₂ concentrations (black lines) because this was superimposed on other kinetic traces (black line *versus* red lines, **Figure 4B**). The second phase was a large decrease in fluorescence intensity; this exponential phase was DMSO₂ concentration-dependent. The observed rate constants analyzed from these kinetic traces were hyperbolically dependent on DMSO₂ concentration with a significant intercept of 2.80 ± 0.12 s⁻¹ (**Figure 4C**). The mechanism was interpreted as a two-step binding process: the first step was DMSO₂ rapid-equilibrium binding to the FMN:DMSMO complex (k_2 and k_{-2} , **Figure 5**) followed by isomerization (k_3 and k_{-3} , **Figure 5**) to be a fully active complex with a decrease in fluorescence intensity. The significant intercept value of 2.8 ± 0.12 s⁻¹ indicated k_{-3} . From the reaction mechanism, K_d (k_{-2}/k_2), k_3 and k_{-3} was obtained from a curve fit to a plot of observed rate constants using Equation 2 to be 1.42 ± 0.08 mM (K_d), 12.7 ± 0.16 s⁻¹ (k_3) and 2.80 ± 0.12 s⁻¹ (k_{-3}), respectively.



Figure 5. The proposed reaction mechanism of DMSO₂ binding to the DMSMO:FMN complex.

After mixing DMSMO:FMN complex with DMSO₂, some of the complex population dissociated shown as an increase in fluorescence intensity (**Figure 3**), whereas the other population binds to DMSO₂ in a two-step process. The first step of the binding process is a rapid equilibrium followed by isomerization to be a fully active complex with a decrease in fluorescence intensity.

Table 1. The rate constants obtained from kinetic analysis using rapid kinetic experiments.

Reactions	Rate constants	Dissociation constants (K_d)
Monooxygenase component		
DMSMO + FMN	$k_i = 4.21 \times 10^6 \text{ M}^{-1} \text{ s}^{-1a}$ $k_r = 92.3 \text{ s}^{-1a}$	$17.4 \pm 0.9 \text{ } \mu\text{M}^b$ $22 \text{ } \mu\text{M}^c$
DMSMO:FMN + DMSO ₂	— $k_3 = 12.7 \pm 0.16 \text{ s}^{-1d}$ $k_{-3} = 2.80 \pm 0.12 \text{ s}^{-1d}$	$1.42 \pm 0.08 \text{ mM}$
DMSMO + FMNH ⁻	—	$4.08 \pm 0.8 \text{ } \mu\text{M}$
DMSMO:FMNH ⁻ + DMSO ₂	—	$6.61 \pm 1 \text{ } \mu\text{M}$
DMSMO:FMNH ⁻ + O ₂	$9.42 \pm 0.71 \times 10^3 \text{ M}^{-1} \text{ s}^{-1e}$ $1.35 \pm 0.06 \times 10^3 \text{ M}^{-1} \text{ s}^{-1e}$	
DMSMO:FMNH ⁻ :DMSO ₂ + O ₂	$4.99 \pm 0.5 \times 10^4 \text{ M}^{-1} \text{ s}^{-1}$	
Reductase component		
DMSR + NADH	$42.7 \text{ M}^{-1} \text{ s}^{-1}$	
Reduced DMSR + O ₂	$4.89 \pm 0.03 \times 10^3 \text{ M}^{-1} \text{ s}^{-1}$	
Monooxygenase + Reductase		
DMSMO:reduced DMSR + O ₂	$1.63 \pm 0.06 \times 10^3 \text{ M}^{-1} \text{ s}^{-1}$	
DMSMO:reduced	$5.1 \pm 0.6 \times 10^4 \text{ M}^{-1} \text{ s}^{-1}$	
DMSR:DMSO ₂ + O ₂		

^aThe rate constants were obtained from simulation (Figure 3B).

^b K_d was obtained from static titration (Figure 3A).

^c K_d was obtained from simulation.

^dThe rate constant from isomerization step in Figure 5.

^eThe oxidation of enzyme showed nonhomogeneous kinetics with fast (~40%) and slow (~60%) populations (Figure 6).

3.1.4 Oxidation of the FMNH⁻:DMSMO complex by oxygen

The oxidation of the DMSMO:FMNH⁻ complex by oxygen was investigated by mixing an anaerobic solution of DMSMO:FMNH⁻ under nitrogen gas in a closed container tonometer with a buffer with various oxygen concentrations. The reaction kinetics were performed using a stopped-flow spectrophotometer. The FMNH⁻ spectrum in the presence of DMSMO showed a perturbation with an increase in extinction at 340 – 400 nm (red line, **Figure 6A**) compared with the free FMNH⁻ spectrum (dotted-black line, **Figure 6A**). The oxidation reaction was monitored from 300–700 nm (5 nm wavelength intervals). The absorbance change showed an increase in absorbance from the reduced to the oxidized flavin (blue line, **Figure 6A**) without the known C4a-hydroperoxyflavin reactive intermediate. The oxidation by O₂ demonstrated two exponential phases. At 0.13 mM oxygen (blue line, **Figure 6B**), the first phase (1 ms–1 s) was an increase in absorbance at 445 nm that was 40% of the total absorbance change. The second phase (1–100 s) was 60% of the total absorbance change (blue line, **Figure 6B**). The observed rate constants of both phases were linearly dependent on the various oxygen concentrations (inset in **Figure 6B**). The bimolecular rate constant for the fast and slow enzyme populations obtained from the slope of the plot (inset in **Figure 6B**) was $9.42 \pm 0.71 \times 10^3 \text{ M}^{-1} \text{ s}^{-1}$ and $1.35 \pm 0.06 \times 10^3 \text{ M}^{-1} \text{ s}^{-1}$, respectively (Table 1). The evidence for the oxidation of the FMNH⁻:DMSMO complex, and not oxidation of the free FMNH⁻, was from a comparison of the control experiments of the oxidation of free FMNH⁻ with the same oxygen concentrations (**Figure 6C**). The kinetic traces also indicated two exponential phases with different kinetic properties. The oxidation of free FMNH⁻ in both exponential phases was faster than in complex with DMSMO.

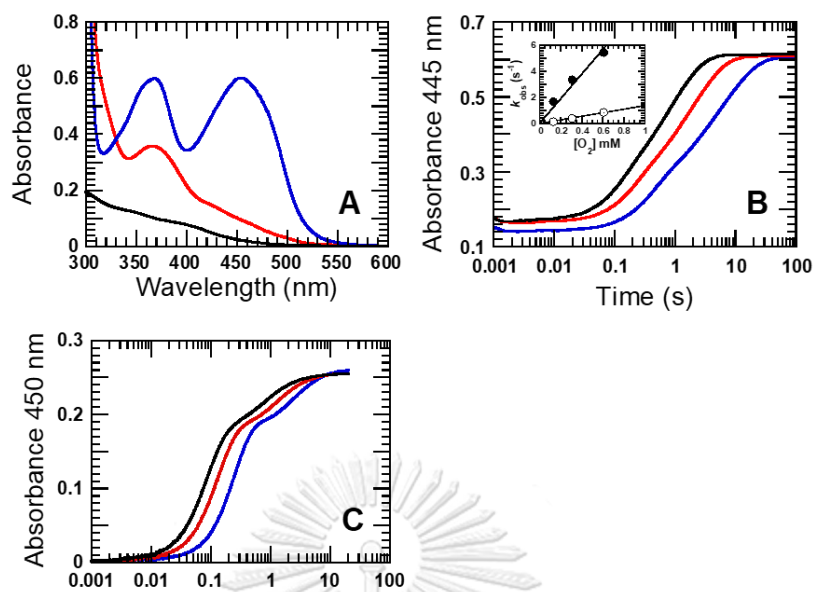


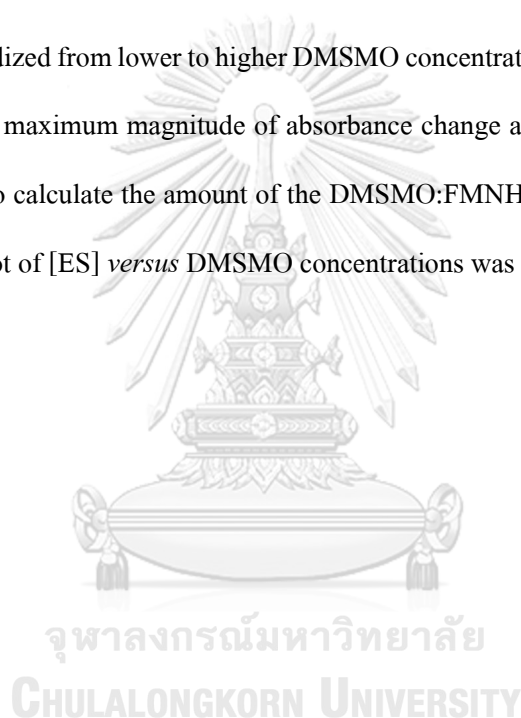
Figure 6. Oxidation of reduced FMN (FMNH^-) in presence of DMSMO. (A) Blue line: the oxidized spectrum of FMNH^- in the presence of $300 \mu\text{M}$ DMSMO. Red line: the reduced spectrum of FMNH^- in the presence of $300 \mu\text{M}$ DMSMO. Black line: the reduced spectrum of free FMNH^- . Both were stoichiometrically reduced using dithionite in anaerobic condition. (B) $56 \mu\text{M}$ FMNH^- and $300 \mu\text{M}$ DMSMO solution was mixed with buffer equilibrated with 0.13 (blue), 0.31 (red) and 3.1 (black) mM oxygen. The reactions were monitored at 445 nm for FMN bound DMSMO oxidation. Inset B is the plot of the observed rate constants (k_{obs}) versus oxygen concentrations. (C) $56 \mu\text{M}$ free FMNH^- solution was mixed with buffer equilibrated with 0.13 (blue), 0.31 (red) and 3.1 (black) mM oxygen. The reactions were monitored at 450 nm for FMN oxidation.

Reaction was performed in 50 mM potassium phosphate pH 7.0 at 25°C using stopped-flow spectrophotometer. All concentrations as described were after mixing.

3.1.5 Binding of monooxygenase to reduced FMN (FMNH^-)

The binding of DMSMO to FMNH^- was observed by absorption spectral perturbation (red line, **Figure 7A**). The rapid kinetics for the oxidation of the FMNH^- :DMSMO complex by oxygen also demonstrated different results from free FMNH^- . This experiment was to investigate how fast the binding of FMNH^- to DMSMO was compared with free FMNH^- oxidation. A different mixing

was performed by the oxidation of pre-equilibrated FMNH^- with DMSMO in air-saturated buffer (blue line, **Figure 7A**), and compared with the kinetic trace from mixing free FMNH^- with DMSMO in air-saturated buffer (red line, **Figure 7A**). The kinetic traces for enzyme oxidation at 445 nm were very similar, indicating that DMSMO binds to FMNH^- very fast before the oxidation of free FMNH^- occurs. Therefore, the K_d for FMNH^- binding to DMSMO could be determined by mixing FMNH^- with various DMSMO concentrations in air-saturated buffer. The dotted-blue line trace (**Figure 7B**) showed the oxidation of free FMNH^- . The FMNH^- in complex with the enzyme was more slowly oxidized from lower to higher DMSMO concentrations (from upper to lower solid lines, **Figure 7B**). A maximum magnitude of absorbance change at 0.6 s using the dotted line as reference was used to calculate the amount of the DMSMO: FMNH^- complex (ES). The K_d value obtained from the plot of [ES] versus DMSMO concentrations was $4.1 \pm 0.8 \mu\text{M}$ (**Figure 7C**).



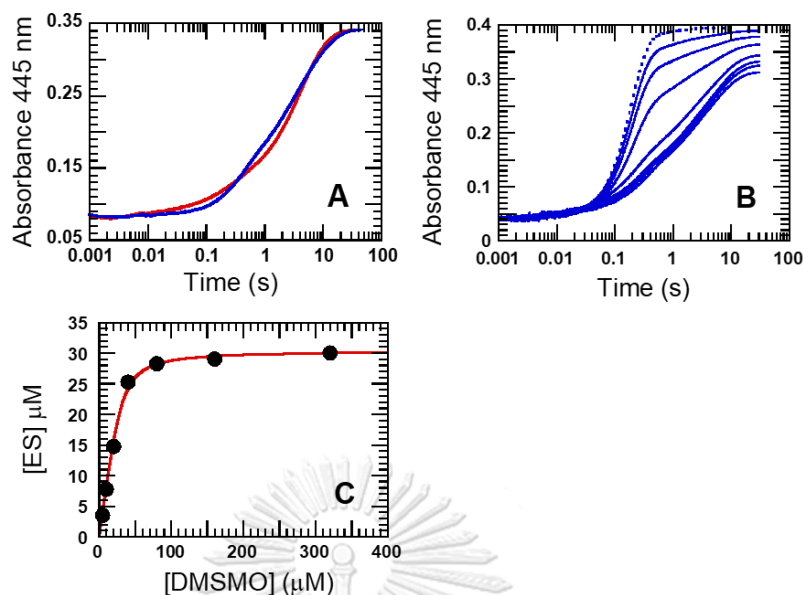


Figure 7. The binding of reduced FMN (FMNH^-) to DMSMO. Alternate mixing experiments between FMNH^- and DMSMO were performed. (A) Blue line: Pre-equilibrated $56 \mu\text{M}$ of FMNH^- and $300 \mu\text{M}$ DMSMO solution mixed with air-saturated buffer. Red line: Same FMNH^- solution was mixed with $300 \mu\text{M}$ DMSMO in air-saturated buffer. (B) $30 \mu\text{M}$ FMNH^- solution was mixed with $10, 20, 40, 80, 160, 320$ and $640 \mu\text{M}$ DMSMO in air-saturated buffer. The dotted-line was the kinetic trace from oxidation of free FMNH^- . The solid lines from the uppermost to the lowest kinetic trace were in the presence of the various DMSMO from the lowest to the highest concentrations as described above. (C) The absorbance change at 0.6 s from the kinetic traces in (B) was used to calculate the FMNH^- :DMSO complex ($[\text{ES}]$) concentrations. The $[\text{ES}]$ concentrations were plotted against the DMSMO concentrations to determine the dissociation constant for binding of FMNH^- to DMSMO.

The reactions were performed in 50 mM potassium phosphate $\text{pH } 7.0$ at 25°C using stopped-flow spectrophotometer. All concentrations as described were after mixing. Oxidation of free FMN and enzyme bound FMN was monitored at 445 nm .

3.1.6 Oxidation of the FMNH^- :DMSMO complex in the presence of DMSO_2

Oxidation of the $\text{DMSMO}:\text{FMNH}^-$ complex by oxygen in the presence of DMSO_2 was performed using rapid kinetics. Scanning the absorbance change from reduced to oxidized enzyme

in the presence of substrate from 300–700 nm did not detect the C4a-hydroperoxyflavin intermediate. The pre-equilibrated DMSMO, oxidized FMN and DMSO₂ to form a ternary complex could not reduce FMN by sodium hydrosulfite. The electrons from sodium hydrosulfite may have reduced 5 mM DMSO₂ instead of flavin because the reduction of FMN using sodium hydrosulfite without substrate had been carried out successfully. Therefore, DMSO₂ had to be separated into the oxygenated buffer and then mixed with the DMSMO/FMN solution. However, it was necessary to demonstrate that DMSO₂ could bind to the DMSMO:FMNH⁻ complex fast enough before reacting with oxygen. The DMSMO and FMN mixture was stoichiometrically reduced in a tonometer attached with a Michel-Miller adapter, and then an anaerobic DMSO₂ solution was transferred to the tonometer under positive nitrogen gas pressure through a long needle gas-tight syringe incorporated with a microtitrator. The ternary complex solution was mixed with air-saturated buffer. The kinetic trace of flavin oxidation at 445 nm (red line, **Figure 8A**) was superimposed with the blue line, which was the kinetic trace from mixing the DMSMO:FMNH⁻ complex with 5 mM DMSO₂ in air-saturated buffer. The results indicated that DMSO₂ binds very fast to DMSMO:FMNH⁻ to form a ternary complex before flavin oxidation. Therefore, the experiments for the oxidation of the FMNH⁻:DMSMO complex in the presence of DMSO₂ were performed by separating DMSO₂ from the FMNH⁻:DMSMO complex.

The DMSMO:FMNH⁻ complex solution was mixed with 5 mM DMSO₂ in various oxygen concentrations (**Figure 8B**). The reactions were monitored by the absorbance change at 445 nm. An increase in absorbance showed a single-exponential phase. The observed rate constants for flavin oxidation were linearly dependent on the oxygen concentrations (inset in **Figure 8B**). The bimolecular rate constant calculated from the slope of the plot was $5.0 \pm 0.5 \times 10^4 \text{ M}^{-1} \text{ s}^{-1}$ (Table 1). The binding of DMSO₂ to DMSMO:FMNH⁻ was observed based on different kinetic properties for oxidation. The ternary complex demonstrated faster oxidation than FMNH⁻:DMSMO, ($5.0 \pm 0.5 \times 10^4 \text{ M}^{-1} \text{ s}^{-1}$ versus $1.4 \pm 0.1 \times 10^3 \text{ M}^{-1} \text{ s}^{-1}$). The dotted-blue line in **Figure 8C** represents the oxidation of DMSMO:FMNH⁻. The solid-blue lines showed that oxidation occurred faster in a

DMSO₂ concentration-dependent manner (**Figure 8C**). A maximum magnitude of absorbance change at 445 nm at 0.1 s using the dotted-blue line as reference was used to calculate the ternary



complex concentrations. The K_d value was obtained from a plot of the ternary complex *versus* the DMSO₂ concentrations at 445 nm as $6.6 \pm 1.0 \mu\text{M}$ (Figure 8D, Table 1).

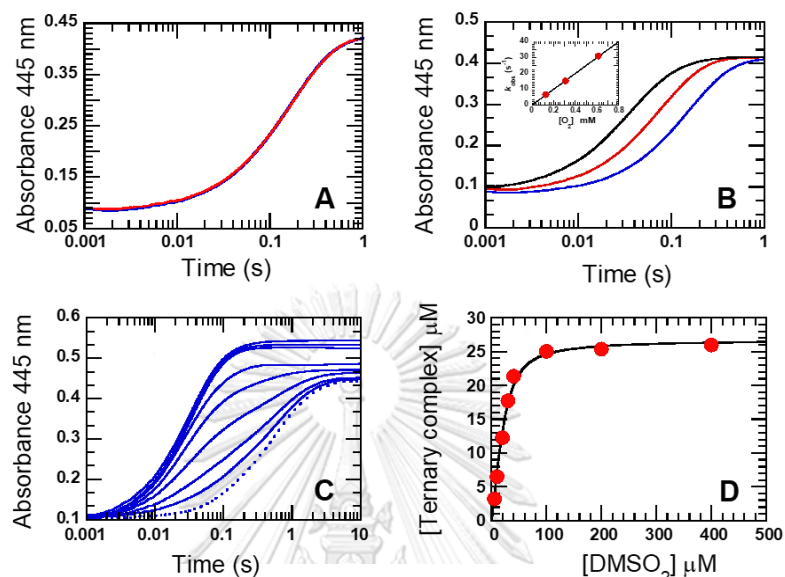
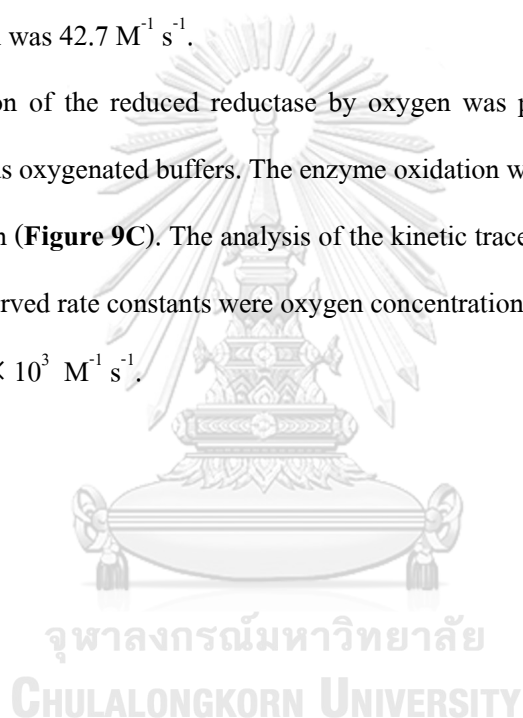


Figure 8. Kinetic oxidation of DMSMO:FMNH⁻ complex in a presence of DMSO₂. Reaction was performed in 50 mM potassium phosphate pH 7.0 at 25 °C using stopped-flow spectrophotometer. All concentrations as described were after mixing. (A) Alternate mixing between DMSO₂ and DMSMO:FMNH⁻ complex. Pre-equilibrated 56 μM FMNH⁻ and 300 μM DMSMO solution was mixed with 5 mM DMSO₂ in air-saturated buffer (blue line). Pre-equilibrated 56 μM FMNH⁻, 300 μM DMSMO and 5 mM DMSO₂ was mixed with air-saturated buffer (Red line) (B) Pre-equilibrated 56 μM FMNH⁻ and 300 μM DMSMO solution was mixed with 5 mM DMSO₂ solutions equilibrated with 0.13 (blue), 0.31 (red) mM and 3.1 (black) mM oxygen. The reactions were monitored at 445 nm for FMN oxidation. Inset B shows the plot of the observed rate constants (k_{obs}) analysed from (B) versus oxygen concentrations. (C) Binding of DMSO₂ to DMSMO:FMNH⁻ complex was investigated by mixing of a 56 μM FMNH⁻ and 300 μM DMSMO solutions with 5 μM, 10 μM, 20 μM, 30 μM, 40 μM, 100 μM, 200, 400 μM DMSO₂ in air-saturated buffer as blue-solid lines. The lowest to uppermost lines were from the lowest to the highest concentrations. Dotted blue line represent the oxidation of DMSMO:FMNH⁻ complex. (D) The [ternary complex] concentrations (calculated from absorbance change at 0.1 s from (C)) were plotted against the DMSO₂ concentrations to determine the dissociation constant for binding of DMSO₂ to DMSMO:FMNH⁻.

3.1.7 Kinetic reduction and oxidation of the reductase component

The reduction of the reductase component was performed by mixing oxidized enzyme with various NADH concentrations under a pseudo-first order condition in an aerobic condition. The enzyme reduction showed a decrease in absorbance at 448 nm (**Figure 9A**). The analysis of the kinetic traces of the reduction demonstrated a single exponential phase. The observed rate constants for flavin reduction were linearly dependent on the NADH concentration (**Figure 9B**). The bimolecular rate constant determined from the slope of the plot of the observed rate constants *versus* NADH concentration was $42.7 \text{ M}^{-1} \text{ s}^{-1}$.

The oxidation of the reduced reductase by oxygen was performed by mixing reduced reductase with various oxygenated buffers. The enzyme oxidation was monitored by an increase in absorbance at 448 nm (**Figure 9C**). The analysis of the kinetic traces showed a single exponential phase where the observed rate constants were oxygen concentration-dependent with a bimolecular rate constant of $4.9 \times 10^3 \text{ M}^{-1} \text{ s}^{-1}$.



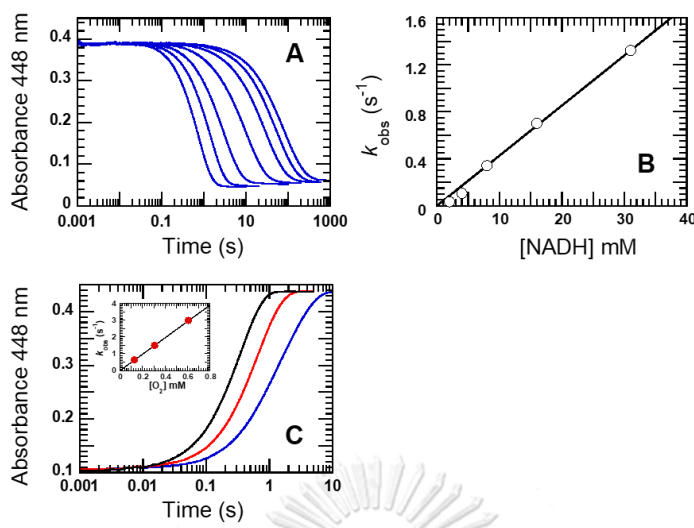


Figure 9. Kinetic reduction and oxidation of the reductase component. (A) 37 μ M DMSR was mixed with 0.5, 1, 2, 4, 8, 16, 31 mM NADH. The blue lines from left to right were according to the lowest to the highest NADH concentrations. (B) A plot of the observed rate constants analyzed from (A) versus NADH concentrations. (C) 37 μ M DMSR solution was stoichiometrically reduced using sodium hydrosulfite. The reduced enzyme was mixed with buffer equilibrated with 0.13 (blue), 0.31 (red) and 3.1 (black) mM. Inset C is the plot of the observed rate constants (k_{obs}) analyzed from (C) versus oxygen concentrations as described above.

Reactions were performed in 50 mM potassium phosphate pH 7.0 at 25 $^{\circ}$ C using stopped-flow spectrophotometer under anaerobic condition. The reactions were monitored at 448 nm for flavin reduction. All concentrations described were after mixing.

CHULALONGKORN UNIVERSITY

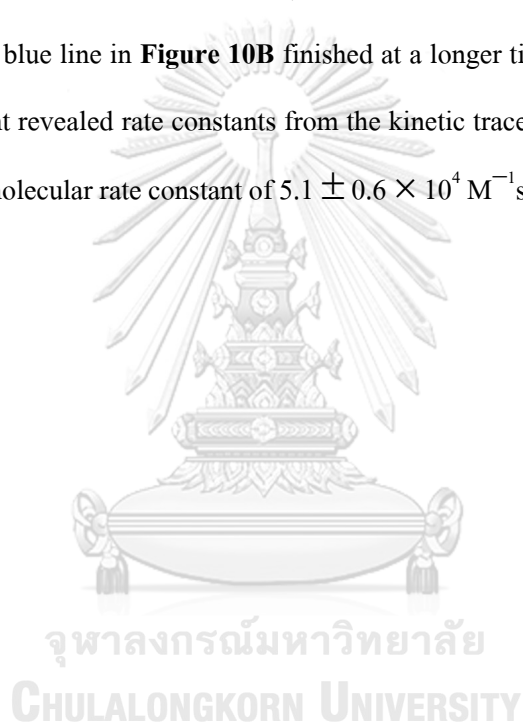
3.1.8 The reduced FMN ($FMNH^{-}$) transfer from the reduced reductase to DMSMO

Mixing the reduced reductase with DMSMO showed a spectrum perturbation with an increased extinction coefficient of 340–400 nm (red line, **Figure 10A**), compared with the reduced reductase spectrum (black line, **Figure 10A**). The observed spectral perturbation was similar to the binding of DMSMO to $FMNH^{-}$ (red line, **Figure 6A**). These results indicated that the $FMNH^{-}$ from the reductase was transferred to the DMSMO active site.

The kinetic properties of flavin oxidation in reduced DMSR with DMSMO mixture was monitored by an absorbance change at 448 nm (**Figure 10B**). The kinetic traces were different from

those of free FMNH⁻ (**Figure 6C**), indicating that all the FMNH⁻ was transferred to DMSMO prior to oxidation. The kinetic analysis of an increase in absorbance at 448 nm demonstrated a single exponential phase. The analysis of the oxygen-dependent observed rate constants from the kinetic traces at 448 nm were linearly dependent with the bimolecular rate constant of $1.6 \pm 0.1 \times 10^3 \text{ M}^{-1} \text{ s}^{-1}$ (inset in **Figure 10B**, Table 1).

In the presence of DMSO₂, the kinetic oxidation was faster than oxidation without DMSO₂. At the same oxygen concentration of 0.13 mM, the reaction of the blue line in **Figure 10C** ended at 1 sec, whereas the blue line in **Figure 10B** finished at a longer time of 50 sec. The analysis of the oxygen-dependent revealed rate constants from the kinetic traces at 448 nm that were linearly dependent with a bimolecular rate constant of $5.1 \pm 0.6 \times 10^4 \text{ M}^{-1} \text{ s}^{-1}$ (inset in **Figure 10C**, Table 1).



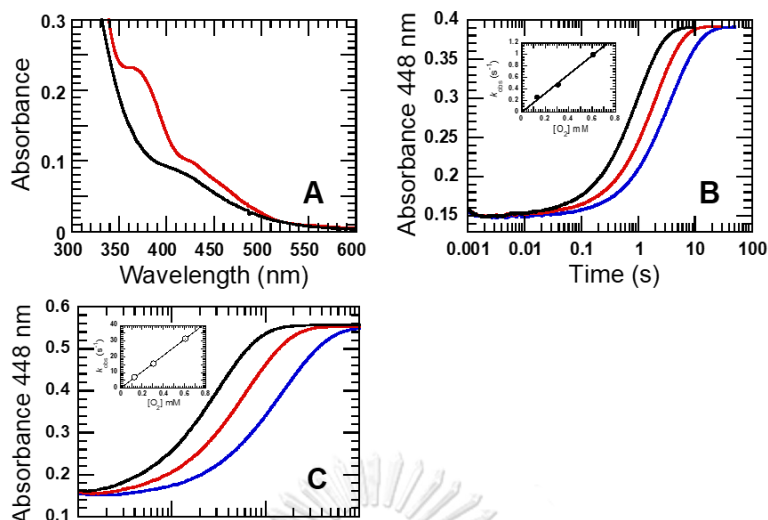


Figure 10. Kinetic oxidation of reduced DMSR and DMSMO complex in absence and presence of DMSO₂. (A) Spectrum of 46 μM DMSR (Black line) and 46 μM DMSR premixed with 300 μM DMSMO solution (Red line) stoichiometrically reduced using sodium hydrosulfite in an anaerobic closed container. The reactions were performed in 50 mM potassium phosphate pH 7.0 at 25 $^{\circ}\text{C}$ using stopped-flow spectrophotometer. All concentrations described were after mixing. The reactions were monitored at 448 nm for flavin oxidation. (B) The solution from A was mixed with 0.13 (blue) mM, 0.31 (red) mM and 1.03 (black) mM oxygenated buffer. The reaction kinetics were monitored by the absorbance change at 448 nm. The observed rate constants (k_{obs}) analyzed from (B) was plotted versus oxygen concentration (inset B). (C) The same solution (A) was mixed with 0.13 mM, 0.31 mM and 1.03 mM oxygenated buffer containing 5 mM substrate DMSO₂. The reactions were monitored at 448 nm for flavin oxidation. The observed rate constants (k_{obs}) analyzed from (C) was plotted versus oxygen concentration (inset C).

3.1.9 Kinetics of the reduced flavin transfer from reduced DMSR to DMSMO

We have already shown that substituting reduced DMSR with reduced FMN in complex with DMSMO provided similar kinetics for oxidation with DMSO₂ (Table 1). In addition, methanesulfinate was identified from the DMSMO in complex with either reduced FMN or reduced DMSR. These results confirmed that the reduced FMN was transferred from DMSR to DMSMO. Therefore, this experiment investigated how quickly the reduced flavin transferred. The experiment

was performed using the double-mixing mode of the stopped-flow spectrophotometer. The reduced DMSR was equilibrated with DMSMO at different times in the first mixing. The solution mixture was mixed with air-saturated buffer to observe the kinetic oxidation of FMNH⁻:DMSMO complex, which was different from the oxidation of reduced DMSR. The oxidation of reduced DMSR ($4.89 \pm 0.03 \times 10^3 \text{ M}^{-1} \text{ s}^{-1}$, Table 1) was faster than the oxidation of reduced DMSR:DMSMO complex ($1.63 \pm 0.06 \times 10^3 \text{ M}^{-1} \text{ s}^{-1}$, Table 1). Therefore, the slower oxidation was used to indicate the FMNH⁻:DMSMO complex. The red line in **Figure 11A** is the control reaction of first mixing the reduced DMSR with anaerobic buffer, and then the reduced enzyme was mixed in an air-saturated buffer (second mixing). The kinetic trace at 448 nm of the flavin oxidation showed that the reaction ended at 18 sec. The green lines in **Figure 11A** are the mixing of reduced DMSR with DMSMO in the first mixing with different equilibration times. The kinetic traces of the equilibration times from 0.01–10 sec were superimposed and their oxidation kinetic traces ended at 80 sec, which were from the FMNH⁻:DMSMO complex. The green lines were also superimposed with the oxidation of pre-equilibrated FMNH⁻:DMSMO (dotted-blue line, **Figure 11A**). The kinetic properties were the same at different equilibration times and the observed rate constant of the reduced FMN transfer from DMSR to DMSMO was estimated using the lowest equilibration time of 0.01 sec to be at least 140 sec^{-1} .

The reduced DMSR was mixed with DMSMO in air-saturated buffer, in a separate syringe, to determine whether the reduced flavin transfer from DMSR to DMSMO occurred in the dead time or not. The black line in **Figure 11B** was from mixing the reduced DMSR with DMSMO prepared in air-saturated buffer in a separate syringe. The kinetic trace for flavin oxidation at 448 nm showed two exponential phases. From 1 msec to 0.8 sec the black line was superimposed with the re-oxidation of reduced DMSR (red line, **Figure 11B**), whereas the black line of 0.8–50 sec was similar to the blue line in **Figure 11B**, which was the trace from mixing the pre-equilibrated reduced DMSR and DMSMO with air-saturated buffer. The results indicated that there was partially a reduced flavin transfer from the reduced DMSR to DMSMO with slower oxidation, whereas the

other population of reduced DMSR was oxidized by oxygen. The magnitude of the absorbance change of the black line (**Figure 11B**) from 1 msec–0.8 sec was 32% of the total absorbance change at 448 nm. Therefore, the other 68% was the oxidation of the reduced FMN:DMSMO complex. The results also demonstrated that oxygen could partially compete to re-oxidize flavin on the reduced DMSR before the reduced flavin is transferred to DMSMO.

The fast transfer of the reduced FMN was possibly from the free reduced FMN released from reduced DMSR prior to mixing with DMSMO. However, the experiment for investigating the amount of reduced FMN released from reduced DMSR was performed using gel filtration sephadex G-10 (see **Methods**). The free reduced FMN released in equilibrium was 166 μM from 400 μM reduced DMSR or only 41.5% that was released as free reduced FMN. Therefore, if only 41.5% was released from DMSR, the oxidation of FMNH^- :DMSMO would show two exponential phases: one would be the rapid binding of the released reduced FMN with DMSMO prior to oxidation by oxygen. This phase would show a magnitude of $\sim 40\%$ of the total absorbance change at 448 nm. The second phase would be the slow release of reduced FMN bound on DMSR with a magnitude of 60% of the total absorbance change at 448 nm. However, the kinetic oxidation of the FMNH^- :DMSMO complex at different equilibration times demonstrated a single exponential phase and was similar to pre-equilibrated FMNH^- :DMSMO (green lines *versus* dotted-blue line, **Figure 11**). The interaction of DMSMO with reduced DMSR might be transient that could trigger the 60% remaining reduced FMN to transfer to DMSMO very fast.

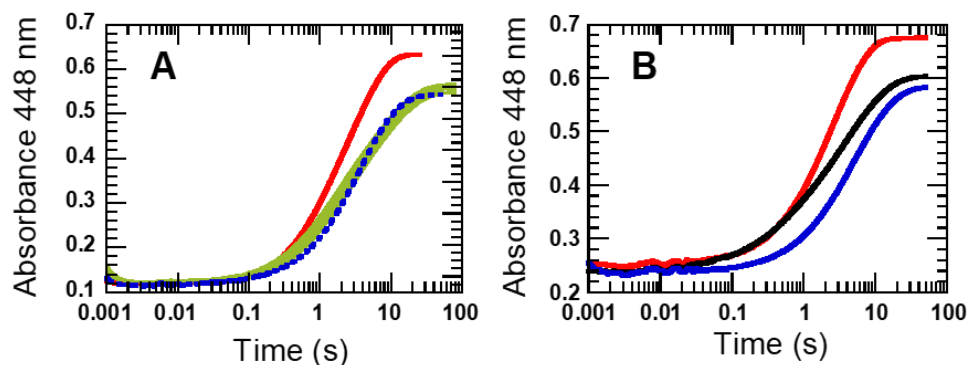


Figure 11. Reduced flavin transfer from reduced DMSR to DMSMO using double-mixing mode of stopped-flow spectrophotometer. (A) reduced DMSR 56 μM solution was mixed with 300 μM DMSMO, both enzymes were prepared in a closed container tonometer under positive nitrogen for anaerobic condition. Red line is a control reaction from the mixing of reduced DMSR with anaerobic buffer (no DMSMO) in the first mixing, and then the solution was mixed with air-saturated buffer. Green lines were from mixing reduced DMSR and DMSMO equilibrated at 0.01 s, 0.02 s, 0.05 s, 0.08 s, 0.1, 0.2s, 1 s, 5 s and 10 s before mixing with air-saturated buffer. Dotted-blue line was a control reaction from mixing pre-equilibrated reduced DMSR and DMSMO with air-saturated buffer. (B) Alternate mixing of reduced DMSR with DMSMO. Red line was from the re-oxidation of 56 μM reduced DMSR with air-saturated buffer. Blue line was from mixing the pre-mixed 56 μM plus 300 μM DMSMO solution with air-saturated buffer. Black line was from mixing 56 μM DMSR with 300 μM DMSMO prepared in air-saturated buffer. The reactions were performed in 50 mM potassium phosphate pH 7.0 at 25 $^{\circ}\text{C}$ using stopped-flow spectrophotometer. All concentrations described were after mixing. The reactions were monitored for flavin oxidation at 448 nm.

3.1.10 Methanesulfinatase analysis from enzyme multiple and single turnover

The product conversion from multiple turnover reactions was performed using concentrations of NADH and DMSO₂ that were higher than those of DMSR and DMSMO under air-saturation. The product from the multiple turnover reactions was analyzed using LC-MS. The percentage of methanesulfinatase in coupled DMSMO and DMSR was only 30% compared with using C₁ reductase 82% (without HPA stimulator) and 96% (with HPA) (Table 2). These findings may be because the reduction of C₁ is much faster than DMSR.

The percent of methanesulfinate using DMSMO and DMSR after adding an extra 56 μM free FMN showed an increase in product that was only 9% (39%) higher than not adding FMN (30%) (Table 2). These results suggested that additional FMN was not important for product formation. This result confirmed the reduced FMN transfer from DMSR.

The percent of methanesulfinate using DMSMO and IIFD, which is a reductase component of the indole 3-monooxygenase system containing FAD as a cofactor, demonstrated very low product formation of 5.7% during multiple turnovers. Although FMN has been demonstrated as a native cofactor, DMSMO might use FADH^- with a low catalytic efficiency. The product was increased to 14.8% when 56 μM free FMN was added to the reaction (Table 2). This result showed that free FMN could accept an electron from FADH^- and transfer it to DMSMO.

The product conversion from single turnover reaction was performed using solutions of reduced FMN or reduced DMSR in the presence of DMSMO under anaerobic condition that were then mixed with air-saturated buffer. The percentage of product formation was based on the starting concentrations of reduced FMN or reduced DMSR. It should be noted that the reducing agents used in the single-turnover reactions have shown a conversion of methanesulfinate to other compounds or a degraded form whose mass could not be detected. Reactions **1** and **2** used 56 μM FMN of which the reducing agents were sodium hydrosulfite and EDTA (photo reduction), respectively (Table 3). The methanesulfinate disappeared when using sodium hydrosulfite, whereas the photoreduction using EDTA showed a lower coupling reaction of 33%, compared with 90.5% from using NADH for reducing DMSR coupled with DMSMO in reaction **10** (Table 3). The control in reaction **3** revealed that oxidized FMN has no effect on methanesulfinate stability.

Table 2. The product conversion of methanesulfinate from enzyme multiple turnover reactions. The reactions contained 56 μM reductase (all types of the reductases), 300 μM DMSMO, 1 mM NADH and 5 mM DMSO_2 . All reactions were performed in 50 mM potassium

phosphate pH 7.0 at 25 °C under air-saturated condition and left for 30 min. The methanesulfinate product was detected using LC-MS equipped with C₁₈ column. The concentrations of methanesulfinate were determined using a calibration curve of a plot of the area under the mass peak versus the standard's concentration. The percentage of methanesulfinate and formaldehyde was calculated based on 1 mM NADH.

Multiple turnover reactions	Methanesulfinate (%)	Formaldehyde (%)
DMSR + DMSMO	30	9.6
DMSR + DMSMO + FMN	39	—
C ₁ ^a + DMSMO	82	—
C ₁ ^a + DMSMO + HPA ^b	96	—
IIFD ^c + DMSMO	5.7	—
IIFD ^c + DMSMO + FMN	14.8	—

^aThe reductase component (FMN bound) of the two-component flavoprotein *p*-hydroxyphenylacetate hydroxylase.

^bThe stimulator of C₁ for reduction by NADH and released FMNH⁻ from C₁.

^cThe reductase component (FAD bound) of the two-component flavoprotein indole 3-monooxygenase.

จุฬาลงกรณ์มหาวิทยาลัย
CHULALONGKORN UNIVERSITY

Table 3. The product conversion of methanesulfinate from single-turnover reactions. All reactions were performed in 50 mM potassium phosphate pH 7.0 at 25 °C. The reactions were

performed using FMN or using the reductase components from other systems: the 56 μM FMNH^- or reduced reductase and 300 μM DMSMO solution was mixed with 5 mM DMSO_2 in air saturation buffer in equal volume. The reducing reagents used for both FMN and DMSR components were specified in the table. The product was analyzed using LC-MS.

Single-turnover reactions	Methanesulfinate (%)
Control reactions	
1. $[\text{FMNH}^- + 56 \mu\text{M methanesulfinate}] + \text{O}_2$ <i>(reduced using sodium hydrosulfite)</i>	not detected
2. $[\text{FMNH}^- + 56 \mu\text{M methanesulfinate} + \text{EDTA}] + \text{O}_2$ <i>(reduced using photoreduction)</i>	33
3. $\text{FMN} + 56 \mu\text{M methanesulfinate}$ <i>(not reduced)</i>	100
4. $56 \mu\text{M H}_2\text{O}_2 + 5 \text{ mM DMSO}_2$	not detected
5. $[\text{FMNH}^- + \text{EDTA}] + [\text{O}_2 + \text{DMSO}_2]$ <i>(reduced using photoreduction)</i>	not detected
Presence of the monooxygenase component	
6. $[\text{FMNH}^- + \text{DMSMO}] + [\text{O}_2 + \text{DMSO}_2]$ <i>(reduced using sodium hydrosulfite)</i>	not detected
7. $[\text{FMNH}^- + \text{DMSMO}] + [\text{O}_2 + \text{DMSO}_2]$ <i>(reduced using EDTA: photoreduction)</i>	15
Presence of the reductase component	
8. $[\text{Reductase} + \text{DMSO}_2] + [\text{O}_2 + \text{DMSO}_2]$ <i>(reduced using NADH)</i>	not detected
Presence of both reductase and monooxygenase	
9. $[\text{DMSR} + \text{DMSMO}] + [\text{O}_2 + \text{DMSO}_2]$ <i>(reduced using sodium hydrosulfite)</i>	84.8
10. $[\text{DMSR} + \text{DMSMO}] + [\text{O}_2 + \text{DMSO}_2]$	90.5

(reduced using NADH)

11. [DMSR + DMSMO + superoxide dismutase (60.5 units)] + [O₂ + DMSO₂] 93.4

(reduced using NADH)

12. [DMSR + DMSMO + catalase (67 μg/ml)] + [O₂ + DMSO₂] 92.3

(reduced using NADH)

3.1.11 Effect of H₂O₂ on product formation

Hydrogen peroxide is one of the reactive oxygen species generated by the oxidation of reduced flavin by oxygen. Mixing hydrogen peroxide directly with DMSO₂ reaction **4** (Table 3) generated no product, including the generated hydrogen peroxide from the oxidation of FMNH⁻ in the presence of 5 mM DMSO₂ in reaction **5**. The photoreaction should generate methanesulfinate if hydrogen peroxide reacts with DMSO₂ because the product is partially affected by EDTA (reaction **2**).

In the presence of DMSMO, using the reducing agents, sodium hydrosulfite and EDTA, reaction **6** and **7** demonstrated in a similar effect to that found in reaction **1** and **2** on methanesulfinate stability. The hydrogen peroxide from the oxidation of reduced DMSR (using NADH) also showed no product in reaction **8**.

In presence of DMSR (reaction **9**), the effect of sodium hydrosulfite was minimized, and the product recovered to 84.8%, compared with using NADH as a reducing agent in reaction **10** where 90.5% of the product formed.

We investigated whether DMSMO used either free form hydrogen peroxide or superoxide radical to incorporate an oxygen atom to DMSO₂. Reactions **11** and **12** were performed using superoxide dismutase and catalase. Neither enzyme demonstrated an effect because the percent coupling of the product was 93.4% and 92.3%, respectively, which were similar to the reactions without either enzyme (reaction **10**).

Table 4. The hydrogen peroxide quantitation from single-turnover reactions. All reactions were performed in 50 mM potassium phosphate pH 7.0 at 25 °C. Air-saturated buffer was used for enzyme re-oxidation. For the reactions using reduced DMSR, the concentrations of DMSR, DMSMO and DMSO₂ was 56 μM, 300 μM, and 5 mM, respectively. For the reactions using reduced C₁ and HPA the concentration was 56 μM and 200 μM, respectively. The percent of hydrogen peroxide was calculated based on either 56 μM of reduced C₁ or reduced DMSR used.

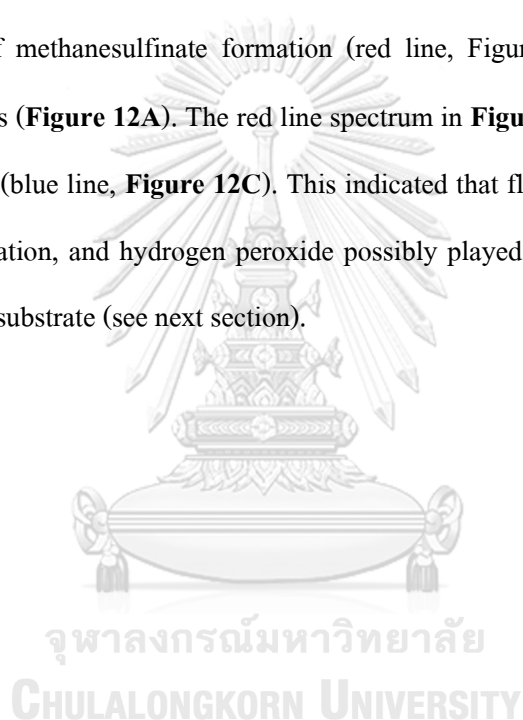
Single-turnover reactions	H ₂ O ₂ (μM)	H ₂ O ₂ (%)
[Reduced C ₁ + HPA] + O ₂	30.2	54
[Reduced C ₁ + HPA + DMSMO] + O ₂	25.8	46
[Reduced C ₁ + HPA + DMSMO] + O ₂ /DMSO ₂	not detected	—
Reduced DMSR + O ₂	48.6 μM	86
[Reduced DMSR + DMSMO] + O ₂	31.3 μM	56
[Reduced DMSR + DMSMO] + O ₂ /DMSO ₂	not detected	—

3.1.12 Determination of the rate constants for monooxygenation using rapid-quenched flow.

The rate constant for the monooxygenation of DMSMO was determined using DMSR as an FMNH⁻ donor. A 56 μM DMSR and 300 μM DMSMO solution was reduced using NADH. The solution containing both enzymes was mixed with 5 mM DMSO₂ in air-saturated buffer. The reactions were quenched using 0.075 M HCl at different time points. The product formed at the different quenching times was analyzed using LC-MS. The concentrations of the product were determined using the area under the mass peak based on a calibration curve. The plot of methanesulfinate concentration *versus* quenched time was fitted with a single exponential phase using Equation 3 to obtain the observed rate constant for monooxygenation of $7.2 \pm 1.2 \text{ s}^{-1}$ (closed-circle red line in **Figure 12A**). The plot was compared with the kinetic trace of flavin oxidation from mixing the reduced DMSR and DMSMO reduced using NADH with air-saturated buffer containing DMSO₂ in a stopped-flow spectrophotometer at the same condition used in the quenched flow experiment. The reaction was monitored at 448 nm. The observed rate constant for flavin

oxidation was $6.2 \pm 0.01 \text{ s}^{-1}$, which was similar to the observed rate constant from the rapid quenched-flow.

A rapid kinetic study using CCD to monitor the change in the oxidation of reduced DMSR in complex with DMSMO without DMSO_2 substrate spectra did not detect an intermediate during enzyme oxidation, only the spectra of the reduced form of flavin was detected (dotted line, **Figure 12B**) to an oxidized form (solid lines, **Figure 12B**). In the presence of substrate, the oxidation of reduced enzyme (black solid line, **Figure 12C**) was compared with the spectrum at 1 sec, which was the end-time of methanesulfinate formation (red line, **Figure 12C**), based on the rapid-quenched flow results (**Figure 12A**). The red line spectrum in **Figure 12C** was not different from fully oxidized flavin (blue line, **Figure 12C**). This indicated that flavin was oxidized at the same rate as product formation, and hydrogen peroxide possibly played an important role for oxygen assimilation into the substrate (see next section).



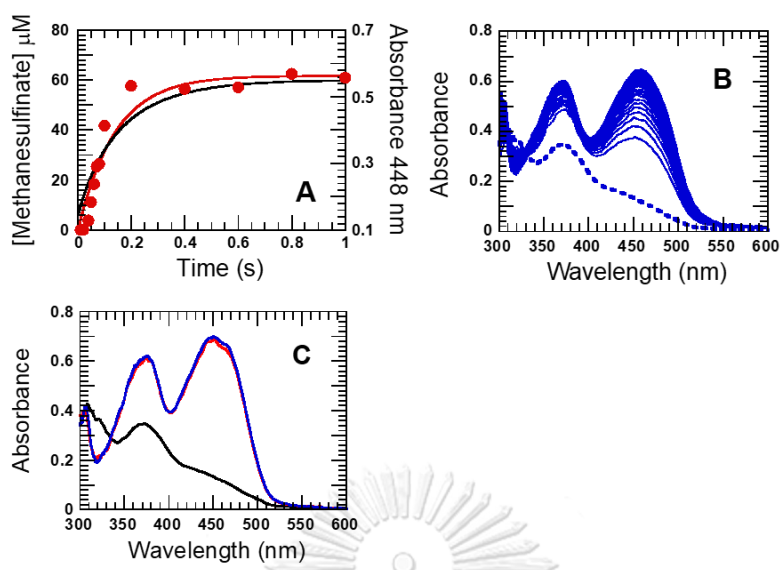


Figure 12. Kinetics and the spectral change for producing methanesulfinatate. (A) Rate constant for producing methanesulfinatate determined using rapid-quenched flow (Red line) vs. rate of flavin oxidation (Black line). 56 μM reduced DMSR and 300 μM DMSMO mixture was prepared. DMSR was stoichiometrically reduced using NADH titration. The reduced DMSR in the presence of DMSMO was mixed with air-saturated buffer containing 5 mM DMSO_2 . The reaction was quenched with 0.075 M HCl at various times. All reactions were performed in 50 mM potassium phosphate pH 7.0 at 25 $^\circ\text{C}$ in an anaerobic glove box. All concentrations described were after mixing. The product was analyzed using LC-MS. The methanesulfinatate concentrations were determined using a standard curve of the area under the mass peak of the methanesulfinatate standard. Dotted-red line represents the methanesulfinatate concentration according to the quenched times. The solid-red line was the curve fit (non-linear algorithm) using one exponential function to obtain the observed rate constant for methanesulfinatate. Black line represents the kinetic trace from mixing the same concentration of reduced DMSR and DMSMO mixed with air-saturated buffer containing 5 mM DMSO_2 . The reaction was performed in a stopped-flow spectrophotometer and monitored an absorbance change at 448 nm. (B) A 56 μM DMSR and 300 μM DMSMO solution was stoichiometrically reduced with NADH and mixed with air-saturated buffer. The reaction was monitored using CCD detector to obtain spectra changing from reduced enzyme (dotted-blue line) to oxidized enzyme. The spectral change was monitored at 0.2 s of interval time until 100 s. (C) The DMSR and DMSMO mixture as (B) was mixed with air-saturated buffer containing 5 mM DMSO_2 . The reaction was monitored using CCD to obtain spectra changing from reduced enzyme (black line) to oxidized enzyme (blue line). The spectral change was monitored at 0.01 sec intervals time up to 3 sec. The red line represents the observed spectrum at 1 s correlated with the time of the end of methanesulfinatate formation.

3.1.13 Quantification of hydrogen peroxide from a single-turnover reaction with or without DMSO_2

The hydrogen peroxide from reduced FMN oxidation in complex with DMSMO was quantified and compared with the same reaction, but in the presence of DMSO_2 . If the hydrogen peroxide from flavin oxidation plays an important role in the catalytic cleavage of dimethyl sulfone into methanesulfinate and formaldehyde, hydrogen peroxide would disappear or be reduced in the presence of DMSO_2 . The C_1 reductase of *p*-hydroxyphenylacetate 3-hydroxylase (HPA) can generate reduced FMN. In the presence of an HPA stimulator, the released reduced FMN will be enhanced. A $56 \mu\text{M}$ C_1 reductase and $300 \mu\text{M}$ DMSMO solution was reduced (blue line, **Figure 13A**) and mixed with air-saturated buffer to the fully oxidized form (red line, **Figure 13A**). The hydrogen peroxide assay reagent (ABTS and horseradish peroxidase) was then added. The oxidized ABTS spectrum with the highest peak at 735 nm and a broad range of 500–1000 nm is seen as a green line (**Figure 13A**). The hydrogen peroxide concentration was determined as $30.2 \mu\text{M}$ or 54% (Table 4). The same experiments using reduced C_1 in the presence of DMSMO (blue line, **Figure 13B**) were mixed with air-saturated buffer to obtain the fully oxidized form (red line, **Figure 13B**). Hydrogen peroxide assay reagent was then added into the reaction (green line, **Figure 13B**). The concentration of hydrogen peroxide decreased to $25.8 \mu\text{M}$ or 46% (Table 4), whereas in the presence of 5 mM DMSO_2 , no oxidized ABTS spectrum was observed (**Figure 13C**).

The same procedure for quantifying hydrogen peroxide was performed using $56 \mu\text{M}$ reduced DMSR (**Figure 13D**). The oxidation of reduced DMSR also generated $48.5 \mu\text{M}$ or 86% hydrogen peroxide (Table 4). In presence of DMSMO (**Figure 13D**), the hydrogen peroxide was decreased to $31.3 \mu\text{M}$ or 56% (Table 4). Similar to the results in **Figure 13C**, hydrogen peroxide was not detected in presence of DMSO_2 (**Figure 13F**). This proves that H_2O_2 is used to attack the DMSO_2 substrate for the oxygenation reaction to form Methanesulfinate.

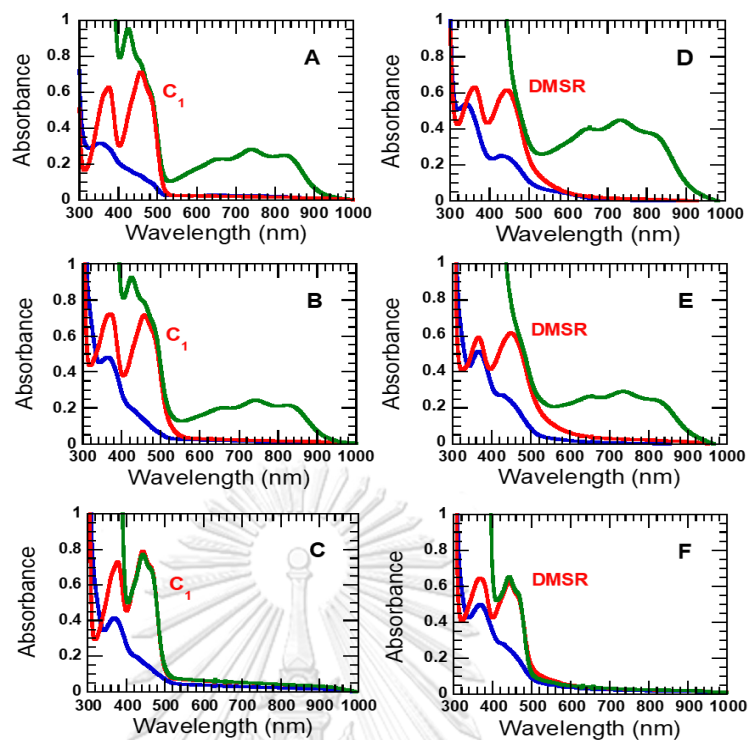


Figure 13. Enzyme utilizing hydrogen peroxide for oxygen assimilation into dimethyl sulfone in

single-turnover reaction. (A) Blue line: $56 \mu\text{M } C_1$ and $200 \mu\text{M HPA}$ solution was stoichiometrically

reduced with NADH. Red line: The reduced enzyme was mixed with air-saturated buffer. Green line:

The enzyme was re-oxidized and 1 mM ABTS and 5 units of HRP solution was mixed with re-oxidized

enzyme. (B) Blue line: $56 \mu\text{M } C_1$, $200 \mu\text{M HPA}$ and $300 \mu\text{M DMSMO}$ solution was reduced as

described in A. Red line: The enzyme mixture was re-oxidized by mixing it with air-saturated buffer.

Green line: The re-oxidized enzyme containing both components was mixed with ABTS and HRP.

(C) Blue line: A $56 \mu\text{M } C_1$, $200 \mu\text{M HPA}$, $300 \mu\text{M DMSMO}$ and 5 mM DMSO_2 solution was

reduced using as described in A. Red line: The enzyme mixture was re-oxidized by mixing it with air-

saturated buffer. Green line: The re-oxidized enzyme containing both components was mixed with

ABTS and HRP. (D) Blue line: $56 \mu\text{M DMSR}$ solution was stoichiometrically reduced with NADH.

Red line: The reduced enzyme was mixed with air-saturated buffer. Green line: The enzyme was re-

oxidized and was hydrogen peroxide formed. A 1 mM ABTS and $5 \text{ units of horseradish peroxidase}$

(HRP) solution was mixed with re-oxidized enzyme. All concentrations as described and spectra were

after mixing. (E) Blue line: $56 \mu\text{M DMSR}$ and $300 \mu\text{M DMSMO}$ solution was reduced using as

described in A. Red line: The enzyme mixture was re-oxidized by mixing it with air-saturated buffer.

Green line: The re-oxidized enzyme containing both components was mixed with ABTS and HRP.

(F) Blue line: A $56 \mu\text{M DMSR}$, $300 \mu\text{M DMSMO}$ and 5 mM DMSO_2 solution was reduced using as

described in A. Red line: The enzyme mixture was re-oxidized by mixing it with air-saturated buffer.

Green line: The re-oxidized enzyme containing both components was mixed with ABTS and HRP.

3.2. Enzyme immobilization

3.2.1 Ni-NTA/H₂N-SiO₂@CoFe₂O₄ characterization

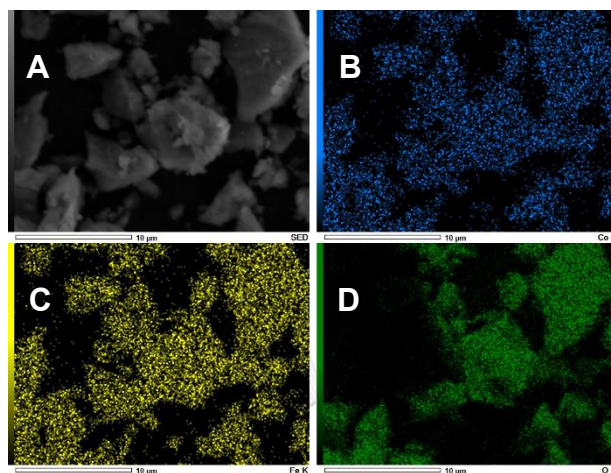


Figure 14. SEM/EDX image of the synthesized Ni-NTA/H₂N-SiO₂@CoFe₂O₄ showing the presence of **B) O**, **C) Fe** and **D) Ni**

The morphology of CoFe₂O₄ nanoparticles was assessed using SEM (**Figure 14**). The images show that the synthesized particles are well uniformed with estimated particles sized of about 500 nm. Energy-dispersive X-ray spectroscopy (EDX) analysis of CoFe₂O₄ confirmed that elements such as Co, Fe, Si, O, C and Ni were uniformly distributed on the surface of the particles (**Figure 14b-d**). The presence of Ni²⁺ indicates the successful surface modification with Ni-NTA.

The X-ray diffraction of the synthesized CoFe₂O₄ and Ni-NTA/H₂N-SiO₂@CoFe₂O₄ corresponds to the crystallized magnetic CoFe₂O₄ plane (JCPDS # 22-1086). The discernable peaks can be indexed to (220), (311), (400), (422), (511) and (440) planes. The diffraction peaks of CoFe₂O₄ and Ni-NTA/H₂N-SiO₂@CoFe₂O are identical to those of the standard magnetic CoFe₂O₄ indicating that the functionalization does not affect the crystal structure of CoFe₂O₄ (**Figure 15**).

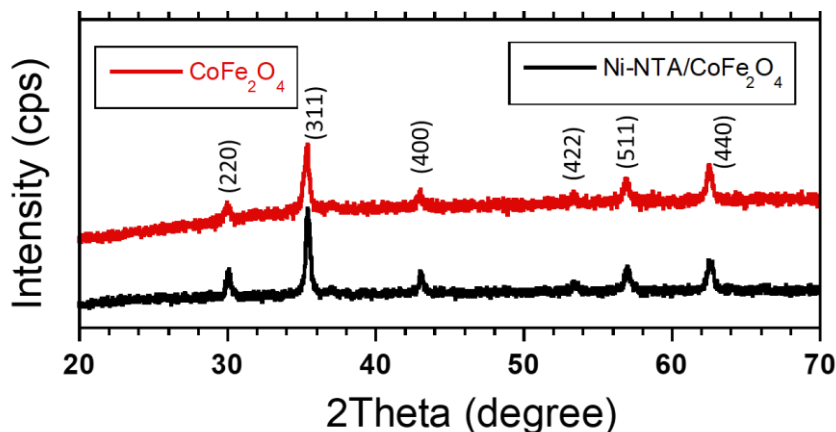


Figure 15. XRD pattern of (A) CoFe_2O_4 and (B) $\text{Ni-NTA}/\text{H}_2\text{N-SiO}_2@\text{CoFe}_2\text{O}_4$.

3.2.2 Immobilization of DMSMO and DMSR onto CoFe_2O_4

To determine the amount of enzyme immobilized onto the nanoparticles, supernatants were collected after incubating both DMSMO and DMSR with the magnetic nanoparticles. Enzyme concentration measured from the collected supernatant will be deemed as the excess enzyme that is not immobilized, once this concentration was subtracted from the initial concentration of enzyme added, the amount of immobilized enzyme was calculated to be approximately $0.6 \mu\text{M}/1 \text{ mg}$ of $\text{Ni-NTA}/\text{H}_2\text{N-SiO}_2@\text{CoFe}_2\text{O}_4$. To study the specificity of Ni-NTA functionalized nanoparticles to the His-tagged DMSMO and DMSR, the immobilized enzyme was eluted and analyzed by SDS-PAGE (**Figure 16**). The sample eluted (lane 4, **Figure 16**) showed only two bands at molecular weight of approximately 42 kDa and 27 kDa, consistent with the weight of DMSMO (41.8 kDa) and DMSR (26.7 kDa), respectively. The size of the elution band shows that DMSR shows a higher affinity for the Ni-NTA functionalized particles when compared to DMSMO.

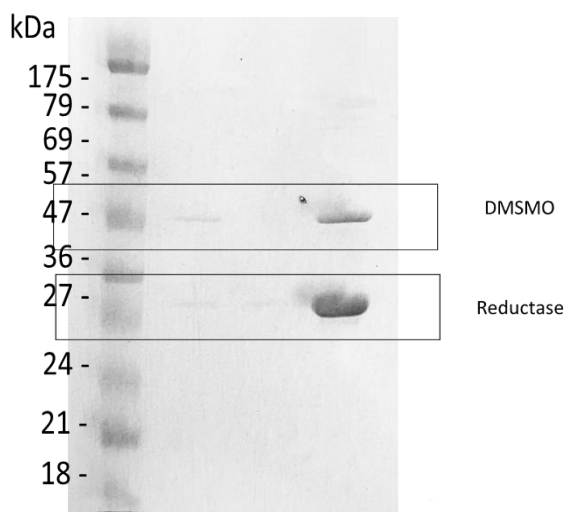


Figure 16. SDS-PAGE (12%) of immobilized DMSMO and DMSR. Lane 1: molecular weight markers, Lane 2: supernatant collected after incubation, Lane 3: wash collected, Lane 4: eluted solution.

3.3.3 Efficiency of immobilized enzyme

To determine the effect of different immobilization types on the enzyme performance, separate immobilization and co-immobilization was prepared and the initial rate was compared to the free DMSMO and DMSR system. The same concentration of enzymes was used for all three types of reactions. The initial rate of each type is shown in Table 4, the results show that the free enzyme system shows the fastest initial rate at $4.23 \pm 0.5 \mu\text{M min}^{-1}$, while the separate immobilization shows a decrease in half of the initial rate at $2.61 \pm 0.4 \mu\text{M min}^{-1}$ and the co-immobilization shows the slowest initial rate at $1.21 \pm 0.1 \mu\text{M min}^{-1}$.

Table 5. The initial rate obtained from multiple turnover reaction

Multiple-turnover reactions	Initial rate ($\mu\text{M min}^{-1}$)
Separate immobilization	2.61 ± 0.4
Co-immobilization	1.21 ± 0.1
Free enzyme	4.23 ± 0.5

3.3.4 Stability of immobilized enzyme

Enzyme efficiencies are greatly affected by the storage environment and environment the reaction occurs. Normally, enzymes are stored at $-80\text{ }^{\circ}\text{C}$, the activity of free DMSMO and DMSR stored at $4\text{ }^{\circ}\text{C}$ was seen to be significantly decreased to about 50% after five days of storage. Immobilization of the enzymes was shown to drastically improve and prolong the activity of the enzyme as the activity remained higher than 50% until day 8 of storage at $4\text{ }^{\circ}\text{C}$ (**Figure 17a**).

For temperature and pH stability, it could be seen that the activity of co-immobilized DMSMO and DMSR was at its peak at pH7.0 and temperature of $30\text{ }^{\circ}\text{C}$. When pH is below 7 and temperature rises above $30\text{ }^{\circ}\text{C}$, it can be seen that the co-immobilized enzyme retains significantly higher activity when compared to the free enzyme (**Figure 17b-c**). Denaturation of enzyme in acidic conditions and temperature of $50\text{ }^{\circ}\text{C}$ can be observed from the precipitation formed. The immobilized DMSMO and DMSR show good reusability, retaining high activity for up to 5 cycles, the activity starts to decrease after 6 cycles onward (**Figure 17d**).

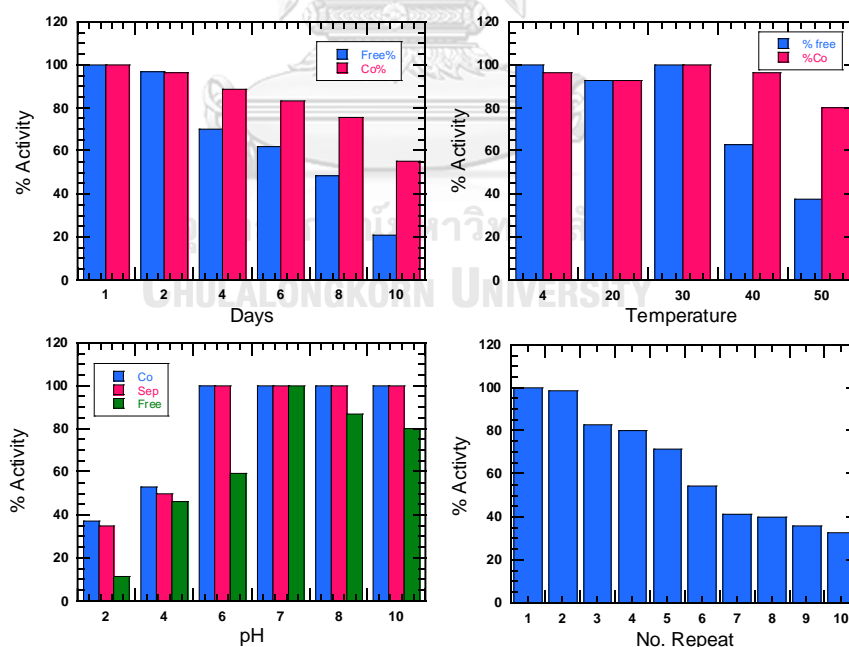


Figure 17. Stability of immobilized DMSMO and DMSR. Activity percentage of the same concentration of free and immobilized enzyme compared for (A) storage at $4\text{ }^{\circ}\text{C}$, (B) temperature ranging from $4\text{--}50\text{ }^{\circ}\text{C}$, (C) pH from 2-10 and (D) activity after recycling of the immobilized enzyme.

4. Discussion and Conclusion

4.1 Mechanistic study of Dimethyl sulfone monooxygenase

The present study has elucidated the kinetic mechanisms of the dimethyl sulfone monooxygenase system, a two-component flavin dependent monooxygenase from *A. baumannii* comprising a monooxygenase (DMSMO) and a reductase (DMSR). The functional studies demonstrated that the catalytic addition of molecular oxygen into the DMSO₂ substrate produced methanesulfinate and formaldehyde. Our study also established a method for identifying methanesulfinate using quadrupole LC-MS. The rapid kinetic study using stopped-flow indicated that no flavin adduct intermediate was involved in the monooxygenation subsequent to substrate cleavage. The results from single-turnover reactions revealed that the H₂O₂ was fully used when dimethyl sulfone was present. H₂O₂ from the oxidation of reduced FMN on DMSMO plays an important role in the catalytic cleavage of dimethyl sulfone to methanesulfinate and formaldehyde. Rapid quenched-flow demonstrated that the observed rate constant for methanesulfinate formation was almost the same as the rate constant for the oxidation of FMNH⁻ bound DMSMO. Therefore, the monooxygenation step using H₂O₂ was very fast, and was limited by the flavin oxidation step.

The purification of DMSMO revealed that ~37% of oxidized FMN was in the bound form. The results from both the static and kinetic binding of DMSMO to oxidized FMN using fluorescent also revealed fast binding with a K_d of 17.4 μM (Figure 2A, Figure 3 and Table 1). The oxygenase component from other two-component flavoproteins, such as C₂ from *p*-hydroxyphenylacetate hydroxylase from *A. baumannii* (Sucharitakul et al., 2007), styrene monooxygenase (Morrison et al., 2013), and dechlorinating flavin-dependent monooxygenase (HadA) (Pimviriyakul et al., 2017) have very low to no binding to the oxidized form of flavin. However, there are some oxygenases or hydroxylases that can bind to oxidized flavin very well, similar to DMSMO, these enzymes include Actinorhodin biosynthesis monooxygenase (ActVA-ORF5) ($K_d = 19.4 \pm 6.3 \mu\text{M}$) (Valton et al., 2004), alkanesulfonate monooxygenase (SsuD) ($K_d = 10.2 \pm 0.4 \mu\text{M}$) (ZHAN ET AL., 2008), and Bacterial luciferase (*Vc*LuxAB) ($K_d = 11 \mu\text{M}$) (TINIKUL ET AL., 2013).

Most of the oxygenase or hydroxylase components have common properties, i.e., fast binding with reduced flavin because the reaction of reduced flavin with oxygen can lead to the formation of many reactive oxygen species (Sucharitakul et al., 2014). In the case of DMSMO, the oxidized FMN bound form also potentially catalyzed DMSO_2 to form products. The multiple-turnover of DMSMO in the presence of NADH and DMSO_2 using IIFD, the reductase from another two-component flavoprotein indole 3-monooxygenase, of which the flavin is FAD also generated a small amount of product. Adding extra $56 \mu\text{M}$ FMN to this mixture increased the product from 5.7% to 14.8%. These results demonstrated that FMN could mediate electron transfer between reduced FAD from IIFD for DMSMO. In the oxidized FMN bound DMSMO population, the free reduced FMN from DMSR likely transfers electrons to oxidized FMN that is already bound in the DMSMO active site for catalysis.

The rapid kinetics study using fluorescence showed quenching from the binding of DMSMO to oxidized FMN followed by more quenching from the binding of dimethyl sulfone to the binary complex (**Figure 4A**). This binding order was assumed to be the same as for reduced FMN. The rapid kinetics study also demonstrated that the binding of DMSO_2 occurs very fast, within the dead time of the stopped-flow machine. The same result was observed when DMSO_2 was added separately. The kinetic trace of flavin oxidation at 445 nm from mixing $\text{FMNH}^-:\text{DMSMO}$ with DMSO_2 in air-saturated buffer was superimposed with the kinetic trace oxidation from the pre-equilibrated ternary complex ($\text{FMNH}^-:\text{DMSMO}:\text{DMSO}_2$) (**Figure 8A**). The fast binding of DMSO_2 is crucial for efficient monooxygenation that is competing with oxidation of $\text{FMNH}^-:\text{DMSMO}$ by oxygen. This enzyme property can explain why the percent methanesulfinate from the single turnover reaction was very high (90.5%) (reaction 10, Table 3). Other oxygenases or hydroxylases of two-component systems, such as C2 and alkanesulfonate monooxygenase (SsuD), demonstrated no interaction of the substrates with the enzymes until the reduced flavin was added (Sucharitakul et al., 2007). The induced conformational change from the

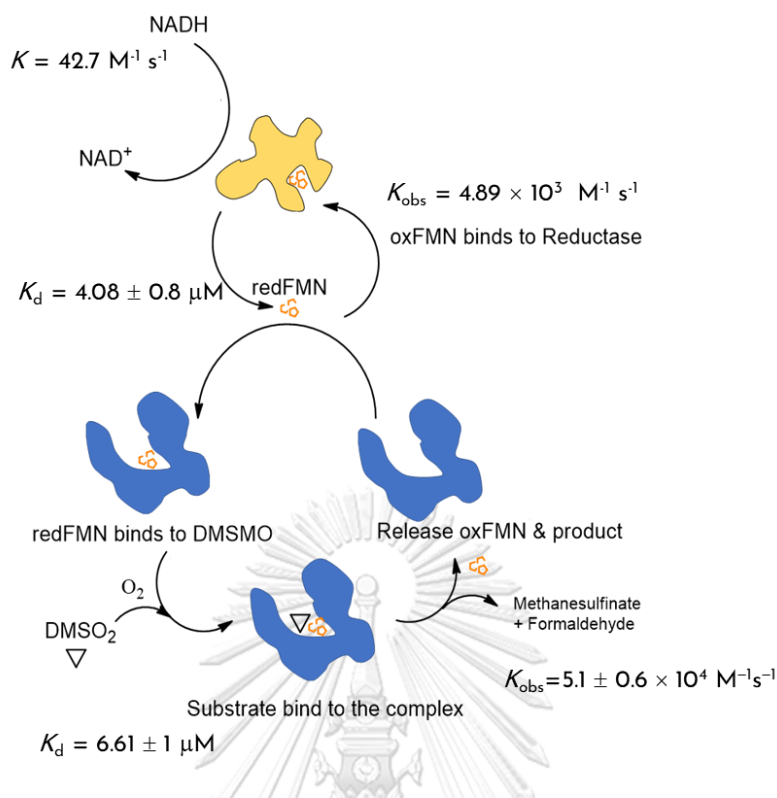
binding of FMNH^- to allow substrate binding to the enzymes was proposed for the SsuD system (Zhan et al., 2008).

The data obtained from the rapid kinetic study using CCD (**Figure 12B**) demonstrated no shifting of the spectra from the reduced to the oxidized state, indicated that C4a-(hydro)peroxyflavin or other flavin-oxygen adduct intermediates were not detected. Another possible intermediate that has been found in other sulfone related monooxygenase systems that resulted in the cleavage of the C-S bond, such as sulfone monooxygenase (DszA) (Sanjoy Adak & Tadhg P. Begley, 2016) and flavoprotein monooxygenase (YxeK) (Matthews et al., 2022) is Flavin-N5-oxide. This flavin adduct was first discovered in EncM-catalyzed 1,3-diketone oxidation (Piano et al., 2017) and is believed to be found in other flavin mediated oxidation reactions where the nucleophilicity of the flavin hydroperoxide needs to be reduced to avoid competing addition to an adjacent electrophilic center. For the reaction catalyzed by DszA, the hydroperoxide intermediate is formed by nucleophilic attack of the flavin peroxide anion on the substrate, which is then reduced, leading to the production of flavin-N5-oxide (S. Adak & T. P. Begley, 2016). Flavin-N5-(hydro)peroxide has distinct spectral characteristics, with the oxidized spectrum slightly shifting toward the longer wavelength (~460–465 nm). This can be seen in enzymes, such as DszA (S. Adak & T. P. Begley, 2016), uracil amide monooxygenase (RutA) (Adak & Begley, 2017), EncM (Teufel et al., 2015), hexachlorobenzene monooxygenase (HcbA1) (Adak & Begley, 2019), and YxeK, which in this case undergoes the formation of Fl_{N5OO} instead of Fl_{N5O} for oxidative catalysis, however, the spectrum shift is the same (Matthews et al., 2022). This spectrum is different from the normal oxidized and reduced flavin spectrum. The spectral change results of the reduced to the oxidized state of DMSR:DMSMO with and without DMSO_2 (**Figure 12B and C**) show normal oxidized flavin spectra (445 nm) that are identical to the spectrum at which product is formed and does not show any spectral changes that resembled those adducts. Because no known intermediates were detected in this system, it is very likely that the reaction does not generate any intermediate, but uses hydrogen peroxide (H_2O_2) instead for the hydroxylation of DMSO_2 .

The H_2O_2 assay in the single-turnover reaction from oxidation of the mixture of reduced DMSR and DMSMO demonstrated no H_2O_2 when DMSO_2 was present. This is strong evidence for the crucial role of H_2O_2 in monooxygenation (**Figure 13E versus 13F, Table 4**). There are several reports about the enzymes that use H_2O_2 generated in an active site reacting with their substrate for monooxygenation, such as L-lysine oxidase/monooxygenase (Trisrivirat et al., 2020), L-lactate monooxygenase (Lockridge et al., 1972), tryptophan 2-monooxygenase (Sobrado & Fitzpatrick, 2003), L-amino acid oxidases (Ullah, 2020), ketone monooxygenase (Britton & Markovetz, 1977) and methanesulfonic acid monooxygenase (MSAMO) (Higgins et al., 1996). The oxidation of reduced DMSR by oxygen produced a high concentration of H_2O_2 (86%). However, when reduced DMSR reacted with DMSO_2 , methanesulfinate was not detected (reaction 8 in **Table 3**). Mixing H_2O_2 directly with DMSO_2 also did not generate methanesulfinate. These results suggested that monooxygenation of the substrate required the DMSMO active site environment. In addition, the percent of H_2O_2 in the presence of DMSMO decreased compared with the H_2O_2 produced from the oxidation of only reduced DMDR (from 86% to 56%) and C_1 reductase (from 54% to 46%) (**Table 4**). The active site of DMSMO might trap H_2O_2 generated from reduced flavin oxidation resulting in 90.5% product generation. The proposed mechanism by which H_2O_2 is generated in the DMSMO active site is that H_2O_2 deprotonation is required to attack the methyl group to produce formaldehyde (**Figure 14**). However, it is unlikely that H_2O_2 is deprotonated in the physiological environment because it has a high $\text{p}K_a$ of 11.6 (St. Laurent et al., 2007). The residues in the DMSMO active site possibly act as a general base (**Figure 14**). The attack by H_2O_2 is proposed to result in substrate cleavage into methanesulfinate and methyl hydroperoxide, which proceeds to form formaldehyde (Barber et al., 1963). MSAMO is an example of an enzyme that undergoes a similar mechanism as DMSMO that is involved in the insertion of H_2O_2 into the carbon atom to form an unstable intermediate, which then spontaneously rearranges to form a sulfite product and formaldehyde (Higgins et al., 1996), where the enzymatic mechanism involves a hydroxyl molecule generated from H_2O_2 . Another study demonstrated that methanesulfinate was the product from the incubation

of dimethyl sulfoxide (DMSO) with a hydroxyl radical (Scaduto, 1995). This mechanism possibly is a part of the H_2O_2 degradation in the DMSMO active site that facilitates the C–S bond cleavage of $DMSO_2$ to produce methanesulfinic acid and formaldehyde (**Figure 13**).

In conclusion, this study has elucidated the kinetic mechanisms of the dimethyl sulfone monooxygenase system (**Scheme 2**). The reductase component (DMSR) slowly reacts with NADH without forming a Michaelis-Menten complex. After reduction, the reduced DMSR is an equilibrium of dissociated free reduced FMN and bound form. However, the results demonstrated that all of the reduced flavin rapidly transferred to DMSMO. A transient complex may trigger the fast release of reduced flavin bound DMSR to DMSMO. The kinetic oxidation of DMSMO in the presence of dimethyl sulfone using CCD to observe spectral changes did not detect any flavin adduct intermediate. The results revealed that the H_2O_2 generated by the oxidation of the reduced FMN in DMSMO is a reactive agent for substrate monooxygenation. The same kinetics of the methanesulfinic acid product formation and flavin oxidation indicates that H_2O_2 rapidly attacks dimethyl sulfone with a rate-limiting flavin oxidation. This study is the first report of the oxygenation mechanism of a two-component flavoprotein catalyzing the oxidative cleavage of dimethyl sulfone to methanesulfinic acid and formaldehyde. Understanding the reaction mechanism from the rapid kinetic study serves as knowledge pertaining to future enzyme structural studies and enzyme engineering for degrading toxic volatile sulfur compounds in wastewater treatments using a biological process.



Scheme 2. Overall reaction mechanism and rate of DMSMO system.

4.2 Co-immobilization of DMSMO and DMSR onto Ni-NTA/ $\text{H}_2\text{N-SiO}_2$ @ CoFe_2O_4

In this study, both DMSMO and DMSR enzyme of the DMSMO system was immobilized onto the Ni-NTA/ $\text{H}_2\text{N-SiO}_2$ @ CoFe_2O_4 nanoparticles by using affinity interaction between the His-tagged enzyme and Ni-NTA functionalized nanoparticles. The synthesized CoFe_2O_4 was surface modified to obtain Ni-NTA/ $\text{H}_2\text{N-SiO}_2$ @ CoFe_2O_4 , characterization of the material was done to determine the morphology and size, as well as to confirm the success of surface modification (**Figure 14 and 15**). Immobilization could be achieved by incubating both enzymes with the support material and separated using a magnet. The immobilized enzyme can be eluted out using high concentration of imidazole, this mimics the purification process done for the purification of DMSMO and DMSR using IMAC SepharoseTM charged with nickel sulfate solution. This suggests that this method of immobilization can be used as a one-step purification process for crude enzymes

without prior purification (Liao et al., 2020), (Barbosa et al., 2015), (Zhao et al., 2021), (Wang et al., 2023).

Previous study on the co-immobilization of two component enzyme system shows that co-immobilized HpaBC system shows the greatest activity when compared to free enzyme or separately immobilized enzyme. This is due to the fact that co-immobilization of two enzymes onto the same carrier brings both enzymes into closer proximity resulting in tighter binding, this allows the FADH^- co-factor to be effectively transferred and bind to the substrate catalytic pocket of HpaB (Liao et al., 2020). However, this does not seem to be the case for this enzyme system as the initial rate obtained from multiple turnovers shows that the immobilized enzyme shows a slightly slower initial rate than that of the free enzyme. This may be due to the uncertain concentration of enzyme being immobilized as the SDS-PAGE from **Figure 16** shows that a higher amount of DMSR was immobilized than DMSMO. This is because DMSR exist in a tetramer in its native form, causing it to have a higher number of His-tagged resulting in higher affinity toward the nanoparticle, and because of the larger size of the tetramer, once DMSR was immobilized, it hindered the site that DMSMO can immobilized onto the support material. This causes the real concentration of the enzyme to be lower when compared to using free enzyme where the exact concentration can be calculated. Moreover, the transfer of co-factor FMNH^- for the DMSMO system does not require the two components to be in close contact with or bind to each other as the result obtained in **Figure 10** shows that high population of FMNH^- was transferred to the DMSMO component through simple diffusion.

Most case studies have shown that immobilization of enzymes increases its stability and durability under different environments (Barbosa et al., 2015; Kondrat et al., 2022; Liao et al., 2020; Souza et al., 2018; Wang et al., 2023; Wang et al., 2022; Yu et al., 2021; Zhao et al., 2021). In this study, the immobilized enzyme shows greater storage life at 4 °C and is able to retain its activity at a wider range of pH and temperature when compared to free enzyme (**Figure 17**). For pH, both immobilized and free enzyme show the maximum relative activity at pH 7-8, the activity drastically

reduced in acidic conditions (pH 2-6). This is because the concentration of H^+ affects the quaternary structure of the enzyme causing it to be denatured, and also affects the dissociation state of the substrate and enzyme (Long et al., 2020; Souza et al., 2018). For thermal durability, the immobilized enzyme was able to retain its activity at higher temperature than that of free enzyme. This is attributed to the increase in rigidity of enzyme when immobilized, preventing the enzyme subunits from dissociation at high temperatures (Zhang et al., 2020). This increase in rigidity is from the chemical bond formed from the physical bonding between the enzyme and support material, which helps protect enzyme from any conformational changes in harsh environment (Bilgin Simsek & Saloglu, 2021).

One of the most interesting properties of immobilized enzyme is its reusability. In free enzyme system, after the reaction is completed, enzyme must be denatured or isolated out of the product using filtration. This means that the enzyme will be discarded and cannot be reused. Immobilization of enzyme onto magnetic nanoparticles not only allows easy separation of enzymes from the product using a magnet but also allow those collected immobilized enzyme to be reused after rinsing with buffer. In this study, the immobilized enzyme can be collected and reused for over 5 cycles and still retain high activity (**Figure 17d**). The decrease in activity after 5 cycles is due to the loss of material during isolating and washing processes, and also from the enzyme detachment from the support material after repeated uses caused by chelating form reduction between Ni^{2+} and His-tagged enzyme (Liao et al., 2020). Apart from the immobilized enzyme reusability, the support material itself can be reused for a high number of cycles as it can be washed and recharged with Ni^{2+} and still retain its affinity toward His-tagged enzyme.

In conclusion, this study has immobilized both DMSMO and DMSR enzymes of the DMSMO system onto Ni-NTA/ $H_2N-SiO_2@CoFe_2O_4$ nanoparticles by specific chelating force between his-tag and Ni^{2+} . The immobilized enzyme shows higher stability at high temperature, wide range of pH and exhibits long-term storage when compared with free enzyme. Moreover, the

immobilized enzyme also exhibits great reusability and ease of separation from the product, which will be beneficial for recycling and industrial applications such as wastewater treatment.



REFERENCES



จุฬาลงกรณ์มหาวิทยาลัย
CHULALONGKORN UNIVERSITY

1. Adak, S., & Begley, T. P. (2016). Dibenzothiophene Catabolism Proceeds via a Flavin-N5-oxide Intermediate. *Journal of the American Chemical Society*, 138(20), 6424-6426. <https://doi.org/10.1021/jacs.6b00583>
2. Adak, S., & Begley, T. P. (2017). RutA-Catalyzed Oxidative Cleavage of the Uracil Amide Involves Formation of a Flavin-N5-oxide. *Biochemistry*, 56(29), 3708-3709. <https://doi.org/10.1021/acs.biochem.7b00493>
3. Adak, S., & Begley, T. P. (2019). Hexachlorobenzene Catabolism Involves a Nucleophilic Aromatic Substitution and Flavin-N5-Oxide Formation. *Biochemistry*, 58(9), 1181-1183. <https://doi.org/10.1021/acs.biochem.9b00012>
4. Alfieri, A., Fersini, F., Ruangchan, N., Prongjit, M., Chaiyen, P., & Mattevi, A. (2007). Structure of the monooxygenase component of a two-component flavoprotein monooxygenase. *Proceedings of the National Academy of Sciences of the United States of America*, 104(4), 1177-1182. <https://doi.org/10.1073/pnas.0608381104>
5. Ambatkar, M., & Usha, M. (2012). Enzymatic treatment of wastewater containing dyestuffs using different delivery systems. *Sci. Rev. Chem. Commun.*, 2.
6. Barber, M., Farren, J., & Linnett, J. W. (1963). The mass spectrometric study of the reaction of methyl radicals with oxygen. *Proceedings of the Royal Society of London. Series A. Mathematical and Physical Sciences*, 274(1358), 306-318. <https://doi.org/doi:10.1098/rspa.1963.0134>
7. Barbosa, O., Ortiz, C., Berenguer-Murcia, Á., Torres, R., Rodrigues, R. C., & Fernandez-Lafuente, R. (2015). Strategies for the one-step immobilization-purification of enzymes as industrial biocatalysts. *Biotechnol Adv*, 33(5), 435-456. <https://doi.org/10.1016/j.biotechadv.2015.03.006>
8. Barnes, I., Hjorth, J., & Mihalopoulos, N. (2006). Dimethyl Sulfide and Dimethyl Sulfoxide and Their Oxidation in the Atmosphere. *Chemical Reviews*, 106(3), 940-975. <https://doi.org/10.1021/cr020529+>
9. Beilke, M. A., Collins-Lech, C., & Sohnle, P. G. (1987). Effects of dimethyl sulfoxide on the oxidative function of human neutrophils. *J Lab Clin Med*, 110(1), 91-96.

10. Bentley, R., & Chasteen, T. G. (2004). Environmental VOSCs—formation and degradation of dimethyl sulfide, methanethiol and related materials. *Chemosphere*, 55(3), 291-317. <https://doi.org/https://doi.org/10.1016/j.chemosphere.2003.12.017>
11. Berresheim, H., Huey, J. W., Thorn, R. P., Eisele, F. L., Tanner, D. J., & Jefferson, A. (1998). Measurements of dimethyl sulfide, dimethyl sulfoxide, dimethyl sulfone, and aerosol ions at Palmer Station, Antarctica. *Journal of Geophysical Research: Atmospheres*, 103(D1), 1629-1637. <https://doi.org/https://doi.org/10.1029/97JD00695>
12. Bilgin Simsek, E., & Saloglu, D. (2021). Exploring the structural and catalytic features of lipase enzymes immobilized on g-C₃N₄: A novel platform for biocatalytic and photocatalytic reactions. *Journal of Molecular Liquids*, 337, 116612. <https://doi.org/https://doi.org/10.1016/j.molliq.2021.116612>
13. Brimblecombe, P. (2015). BIOGEOCHEMICAL CYCLES | Sulfur Cycle. In G. R. North, J. Pyle, & F. Zhang (Eds.), *Encyclopedia of Atmospheric Sciences (Second Edition)* (pp. 187-193). Academic Press. <https://doi.org/https://doi.org/10.1016/B978-0-12-382225-3.00015-3>
14. Britton, L. N., & Markovetz, A. J. (1977). A novel ketone monooxygenase from *Pseudomonas cepacia*. Purification and properties. *Journal of Biological Chemistry*, 252(23), 8561-8566. [https://doi.org/https://doi.org/10.1016/S0021-9258\(19\)75257-0](https://doi.org/https://doi.org/10.1016/S0021-9258(19)75257-0)
15. Chasteen, T. G., & Bentley, R. (2004). Volatile Organic Sulfur Compounds of Environmental Interest: Dimethyl Sulfide and Methanethiol. An Introductory Overview. *Journal of Chemical Education*, 81(10), 1524. <https://doi.org/10.1021/ed081p1524>
16. Chenprakhon, P., Pimviriyakul, P., Tongsook, C., & Chaiyen, P. (2020). Chapter Ten - Phenolic hydroxylases. In P. Chaiyen & F. Tamanoi (Eds.), *The Enzymes* (Vol. 47, pp. 283-326). Academic Press. <https://doi.org/https://doi.org/10.1016/bs.enz.2020.05.008>
17. Csarman, F., Wohlschlager, L., & Ludwig, R. (2020). Chapter Fifteen - Cellobiose dehydrogenase. In P. Chaiyen & F. Tamanoi (Eds.), *The Enzymes* (Vol. 47, pp. 457-489). Academic Press. <https://doi.org/https://doi.org/10.1016/bs.enz.2020.06.002>
18. Cui, J., Zhao, Y., Liu, R., Zhong, C., & Jia, S. (2016). Surfactant-activated lipase hybrid nanoflowers with enhanced enzymatic performance. *Scientific Reports*, 6(1), 27928. <https://doi.org/10.1038/srep27928>

19. de Almeida, J. M., Moure, V. R., Müller-Santos, M., de Souza, E. M., Pedrosa, F. O., Mitchell, D. A., & Krieger, N. (2018). Tailoring recombinant lipases: keeping the His-tag favors esterification reactions, removing it favors hydrolysis reactions. *Scientific Reports*, 8(1), 10000. <https://doi.org/10.1038/s41598-018-27579-8>
20. Eichhorn, E., Davey, C. A., Sargent, D. F., Leisinger, T., & Richmond, T. J. (2002). Crystal Structure of Escherichia coli Alkanesulfonate Monooxygenase SsuD. *Journal of Molecular Biology*, 324(3), 457-468. [https://doi.org/https://doi.org/10.1016/S0022-2836\(02\)01069-0](https://doi.org/https://doi.org/10.1016/S0022-2836(02)01069-0)
21. Ellis, H. R. (2010). The FMN-dependent two-component monooxygenase systems. *Archives of Biochemistry and Biophysics*, 497(1), 1-12. <https://doi.org/https://doi.org/10.1016/j.abb.2010.02.007>
22. Ewing, T. A., Gygli, G., Fraaije, M. W., & van Berkel, W. J. H. (2020). Chapter Four - Vanillyl alcohol oxidase. In P. Chaiyen & F. Tamanoi (Eds.), *The Enzymes* (Vol. 47, pp. 87-116). Academic Press. <https://doi.org/https://doi.org/10.1016/bs.enz.2020.05.003>
23. Gadda, G. (2020). Chapter Six - Choline oxidases. In P. Chaiyen & F. Tamanoi (Eds.), *The Enzymes* (Vol. 47, pp. 137-166). Academic Press. <https://doi.org/https://doi.org/10.1016/bs.enz.2020.05.004>
24. Grimble, R. F. (2006). The effects of sulfur amino acid intake on immune function in humans. *J Nutr*, 136(6 Suppl), 1660s-1665s. <https://doi.org/10.1093/jn/136.6.1660S>
25. Habe, H., Kouzuma, A., Endoh, T., Omori, T., Yamane, H., & Nojiri, H. (2007). Transcriptional regulation of the sulfate-starvation-induced gene *sfnA* by a σ^{54} -dependent activator of *Pseudomonas putida*. *Microbiology*, 153(9), 3091-3098. <https://doi.org/https://doi.org/10.1099/mic.0.2007/008151-0>
26. He, X., & Slupsky, C. M. (2014). Metabolic Fingerprint of Dimethyl Sulfone (DMSO₂) in Microbial–Mammalian Co-metabolism. *Journal of Proteome Research*, 13(12), 5281-5292. <https://doi.org/10.1021/pr500629t>
27. Higgins, T. P., Davey, M., Trickett, J., Kelly, D. P., & Murrell, J. C. (1996). Metabolism of methanesulfonic acid involves a multicomponent monooxygenase enzyme. *Microbiology*, 142(2), 251-260. <https://doi.org/https://doi.org/10.1099/13500872-142-2-251>

28. Hutt, L. P. (2018). Bacterial Metabolism of C 1 Sulfur Compounds Rich Boden and.
29. Jortzik, E., Wang, L., Ma, J., & Becker, K. (2014). Flavins and Flavoproteins: Applications in Medicine. In S. Weber & E. Schleicher (Eds.), *Flavins and Flavoproteins: Methods and Protocols* (pp. 113-157). Springer New York. https://doi.org/10.1007/978-1-4939-0452-5_7
30. Kertesz, M. A. (2000). Riding the sulfur cycle--metabolism of sulfonates and sulfate esters in gram-negative bacteria. *FEMS Microbiol Rev*, 24(2), 135-175. [https://doi.org/10.1016/s0168-6445\(99\)00033-9](https://doi.org/10.1016/s0168-6445(99)00033-9)
31. Kim, Y. H., Kim, D. H., Lim, H., Baek, D. Y., Shin, H. K., & Kim, J. K. (2009). The anti-inflammatory effects of methylsulfonylmethane on lipopolysaccharide-induced inflammatory responses in murine macrophages. *Biol Pharm Bull*, 32(4), 651-656. <https://doi.org/10.1248/bpb.32.651>
32. Kino, K., Murakami-Nitta, T., Oishi, M., Ishiguro, S., & Kirimura, K. (2004). Isolation of dimethyl sulfone-degrading microorganisms and application to odorless degradation of dimethyl sulfoxide. *Journal of Bioscience and Bioengineering*, 97(1), 82-84. [https://doi.org/https://doi.org/10.1016/S1389-1723\(04\)70171-1](https://doi.org/https://doi.org/10.1016/S1389-1723(04)70171-1)
33. Kondrat, S., Krauss, U., & von Lieres, E. (2022). Enzyme co-localisation: Mechanisms and benefits. *Current Research in Chemical Biology*, 2, 100031. <https://doi.org/https://doi.org/10.1016/j.crchbi.2022.100031>
34. Krajewska, B. (2004). Application of chitin- and chitosan-based materials for enzyme immobilizations: a review. *Enzyme and Microbial Technology*, 35(2), 126-139. <https://doi.org/https://doi.org/10.1016/j.enzmictec.2003.12.013>
35. Liao, J., Han, S., Li, X., He, J., Secundo, F., & Liang, H. (2020). Co-immobilization of two-component hydroxylase monooxygenase by functionalized magnetic nanoparticles for preserving high catalytic activity and enhancing enzyme stability. *International Journal of Biological Macromolecules*, 164, 3163-3170. <https://doi.org/10.1016/j.ijbiomac.2020.08.182>
36. Lienhart, W.-D., Gudipati, V., & Macheroux, P. (2013). The human flavoproteome. *Archives of Biochemistry and Biophysics*, 535(2), 150-162. <https://doi.org/https://doi.org/10.1016/j.abb.2013.02.015>

37. Lockridge, O., Massey, V., & Sullivan, P. A. (1972). Mechanism of Action of the Flavoenzyme Lactate Oxidase. *Journal of Biological Chemistry*, 247(24), 8097-8106. [https://doi.org/https://doi.org/10.1016/S0021-9258\(20\)81814-6](https://doi.org/https://doi.org/10.1016/S0021-9258(20)81814-6)
38. Long, J., Pan, T., Xie, Z., Xu, X., & Jin, Z. (2020). Co-immobilization of β -fructofuranosidase and glucose oxidase improves the stability of Bi-enzymes and the production of lactosucrose. *LWT*, 128, 109460. <https://doi.org/https://doi.org/10.1016/j.lwt.2020.109460>
39. Macheroux, P., Kappes, B., & Ealick, S. E. (2011). Flavogenomics – a genomic and structural view of flavin-dependent proteins. *The FEBS Journal*, 278(15), 2625-2634. <https://doi.org/https://doi.org/10.1111/j.1742-4658.2011.08202.x>
40. Martin, C., Binda, C., Fraaije, M. W., & Mattevi, A. (2020). Chapter Three - The multipurpose family of flavoprotein oxidases. In P. Chaiyen & F. Tamanoi (Eds.), *The Enzymes* (Vol. 47, pp. 63-86). Academic Press. <https://doi.org/https://doi.org/10.1016/bs.enz.2020.05.002>
41. Massey, V. (2000). The Chemical and Biological Versatility of Riboflavin. *Biochemical Society Transactions*, 28(4), 283-296. <https://doi.org/10.1042/bst0280283>
42. Mateo, C., Palomo, J. M., Fernandez-Lorente, G., Guisan, J. M., & Fernandez-Lafuente, R. (2007). Improvement of enzyme activity, stability and selectivity via immobilization techniques. *Enzyme and Microbial Technology*, 40(6), 1451-1463. <https://doi.org/https://doi.org/10.1016/j.enzmictec.2007.01.018>
43. Matthews, A., Saleem-Batcha, R., Sanders, J. N., Stull, F., Houk, K. N., & Teufel, R. (2020). Aminoperoxide adducts expand the catalytic repertoire of flavin monooxygenases. *Nature Chemical Biology*, 16(5), 556-563. <https://doi.org/10.1038/s41589-020-0476-2>
44. Matthews, A., Schönfelder, J., Lagies, S., Schleicher, E., Kammerer, B., Ellis, H. R., Stull, F., & Teufel, R. (2022). Bacterial flavoprotein monooxygenase YxeK salvages toxic S-(2-succino)-adducts via oxygenolytic C–S bond cleavage. *The FEBS Journal*, 289(3), 787-807. <https://doi.org/https://doi.org/10.1111/febs.16193>
45. Morrison, E., Kantz, A., Gassner, G. T., & Sazinsky, M. H. (2013). Structure and Mechanism of Styrene Monooxygenase Reductase: New Insight into the FAD-Transfer Reaction. *Biochemistry*, 52(35), 6063-6075. <https://doi.org/10.1021/bi400763h>

46. Pearson, T. W., Dawson, H. J., & Lackey, H. B. (1981). Natural occurring levels of dimethyl sulfoxide in selected fruits, vegetables, grains, and beverages. *J Agric Food Chem*, 29(5), 1089-1091. <https://doi.org/10.1021/jf00107a049>
47. Phintha, A., Prakinee, K., & Chaiyen, P. (2020). Chapter Eleven - Structures, mechanisms and applications of flavin-dependent halogenases. In P. Chaiyen & F. Tamanoi (Eds.), *The Enzymes* (Vol. 47, pp. 327-364). Academic Press. <https://doi.org/https://doi.org/10.1016/bs.enz.2020.05.009>
48. Piano, V., Palfey, B. A., & Mattevi, A. (2017). Flavins as Covalent Catalysts: New Mechanisms Emerge. *Trends Biochem Sci*, 42(6), 457-469. <https://doi.org/10.1016/j.tibs.2017.02.005>
49. Pimviriyakul, P., & Chaiyen, P. (2020a). Chapter One - Overview of flavin-dependent enzymes. In P. Chaiyen & F. Tamanoi (Eds.), *The Enzymes* (Vol. 47, pp. 1-36). Academic Press. <https://doi.org/https://doi.org/10.1016/bs.enz.2020.06.006>
50. Pimviriyakul, P., & Chaiyen, P. (2020b). Chapter Twelve - Flavin-dependent dehalogenases. In P. Chaiyen & F. Tamanoi (Eds.), *The Enzymes* (Vol. 47, pp. 365-397). Academic Press. <https://doi.org/https://doi.org/10.1016/bs.enz.2020.05.010>
51. Pimviriyakul, P., Thotsaporn, K., Sucharitakul, J., & Chaiyen, P. (2017). Kinetic Mechanism of the Dechlorinating Flavin-dependent Monooxygenase HadA*. *Journal of Biological Chemistry*, 292(12), 4818-4832. <https://doi.org/https://doi.org/10.1074/jbc.M116.774448>
52. Ren, S., Li, C., Jiao, X., Jia, S., Jiang, Y., Bilal, M., & Cui, J. (2019). Recent progress in multienzymes co-immobilization and multienzyme system applications. *Chemical Engineering Journal*, 373, 1254-1278. <https://doi.org/https://doi.org/10.1016/j.cej.2019.05.141>
53. Scaduto, R. C. (1995). Oxidation of dmsO and methanesulfinic acid by the hydroxyl radical. *Free Radical Biology and Medicine*, 18(2), 271-277. [https://doi.org/https://doi.org/10.1016/0891-5849\(94\)E0139-A](https://doi.org/https://doi.org/10.1016/0891-5849(94)E0139-A)
54. Schmidt, S., & Bornscheuer, U. T. (2020). Chapter Nine - Baeyer-Villiger monooxygenases: From protein engineering to biocatalytic applications. In P. Chaiyen &

- F. Tamanoi (Eds.), *The Enzymes* (Vol. 47, pp. 231-281). Academic Press.
<https://doi.org/https://doi.org/10.1016/bs.enz.2020.05.007>
55. Serrano, A., Carro, J., & Martínez, A. T. (2020). Chapter Seven - Reaction mechanisms and applications of aryl-alcohol oxidase. In P. Chaiyen & F. Tamanoi (Eds.), *The Enzymes* (Vol. 47, pp. 167-192). Academic Press.
<https://doi.org/https://doi.org/10.1016/bs.enz.2020.05.005>
56. Sheng, Y., Chen, F., Wang, X., Sheng, G., & Fu, J. (2008). Odorous volatile organic sulfides in wastewater treatment plants in Guangzhou, China. *Water Environ Res*, 80(4), 324-330. <https://doi.org/10.2175/106143007x221274>
57. Simó, R. (1998). Trace chromatographic analysis of dimethyl sulfoxide and related methylated sulfur compounds in natural waters. *J Chromatogr A*, 807(2), 151-164.
[https://doi.org/10.1016/s0021-9673\(98\)00086-7](https://doi.org/10.1016/s0021-9673(98)00086-7)
58. Sobrado, P., & Fitzpatrick, P. F. (2003). Identification of Tyr413 as an active site residue in the flavoprotein tryptophan 2-monooxygenase and analysis of its contribution to catalysis. *Biochemistry*, 42(47), 13833-13838. <https://doi.org/10.1021/bi035300i>
59. Souza, C. J. F., Garcia-Rojas, E. E., & Favaro-Trindade, C. S. (2018). Lactase (β -galactosidase) immobilization by complex formation: Impact of biopolymers on enzyme activity. *Food Hydrocolloids*, 83, 88-96.
<https://doi.org/https://doi.org/10.1016/j.foodhyd.2018.04.044>
60. St. Laurent, J. B., de Buzzaccarini, F., De Clerck, K., Demeyere, H., Labeque, R., Lodewick, R., & van Langenhove, L. (2007). B.1.I - Laundry Cleaning of Textiles. In I. Johansson & P. Somasundaran (Eds.), *Handbook for Cleaning/Decontamination of Surfaces* (pp. 57-102). Elsevier Science B.V. <https://doi.org/https://doi.org/10.1016/B978-044451664-0/50003-6>
61. Sucharitakul, J., Chaiyen, P., Entsch, B., & Ballou, D. P. (2006). Kinetic Mechanisms of the Oxygenase from a Two-component Enzyme, p-Hydroxyphenylacetate 3-Hydroxylase from *Acinetobacter baumannii**. *Journal of Biological Chemistry*, 281(25), 17044-17053.
<https://doi.org/https://doi.org/10.1074/jbc.M512385200>
62. Sucharitakul, J., Phongsak, T., Entsch, B., Svasti, J., Chaiyen, P., & Ballou, D. P. (2007). Kinetics of a Two-Component p-Hydroxyphenylacetate Hydroxylase Explain How

- Reduced Flavin Is Transferred from the Reductase to the Oxygenase. *Biochemistry*, 46(29), 8611-8623. <https://doi.org/10.1021/bi7006614>
63. Sucharitakul, J., Tinikul, R., & Chaiyen, P. (2014). Mechanisms of reduced flavin transfer in the two-component flavin-dependent monooxygenases. *Archives of Biochemistry and Biophysics*, 555-556, 33-46. <https://doi.org/https://doi.org/10.1016/j.abb.2014.05.009>
64. Tanner, J. J., Lei, B., Tu, S.-C., & Krause, K. L. (1996). Flavin Reductase P: Structure of a Dimeric Enzyme That Reduces Flavin. *Biochemistry*, 35(42), 13531-13539. <https://doi.org/10.1021/bi961400v>
65. Taylor, K. E., Al-Kassim, L., Bewtra, J. K., Biswas, N., & Taylor, J. (1996). Enzyme-Based Wastewater Treatment: Removal of Phenols by Oxidative Enzymes. In M. Moo-Young, W. A. Anderson, & A. M. Chakrabarty (Eds.), *Environmental Biotechnology: Principles and Applications* (pp. 524-532). Springer Netherlands. https://doi.org/10.1007/978-94-017-1435-8_46
66. Teufel, R., Stull, F., Meehan, M. J., Michaudel, Q., Dorrestein, P. C., Palfey, B., & Moore, B. S. (2015). Biochemical Establishment and Characterization of EncM's Flavin-N5-oxide Cofactor. *Journal of the American Chemical Society*, 137(25), 8078-8085. <https://doi.org/10.1021/jacs.5b03983>
67. Tinikul, R., Chunthaboon, P., Phonbuppha, J., & Paladkong, T. (2020). Chapter Fourteen - Bacterial luciferase: Molecular mechanisms and applications. In P. Chaiyen & F. Tamanoi (Eds.), *The Enzymes* (Vol. 47, pp. 427-455). Academic Press. <https://doi.org/https://doi.org/10.1016/bs.enz.2020.06.001>
68. Tinikul, R., Pitsawong, W., Sucharitakul, J., Nijvipakul, S., Ballou, D. P., & Chaiyen, P. (2013). The Transfer of Reduced Flavin Mononucleotide from LuxG Oxidoreductase to Luciferase Occurs via Free Diffusion. *Biochemistry*, 52(39), 6834-6843. <https://doi.org/10.1021/bi4006545>
69. Tischler, D., Kumpf, A., Eggerichs, D., & Heine, T. (2020). Chapter Thirteen - Styrene monooxygenases, indole monooxygenases and related flavoproteins applied in bioremediation and biocatalysis. In P. Chaiyen & F. Tamanoi (Eds.), *The Enzymes* (Vol. 47, pp. 399-425). Academic Press. <https://doi.org/https://doi.org/10.1016/bs.enz.2020.05.011>

70. Trisrivirat, D., Lawan, N., Chenprakhon, P., Matsui, D., Asano, Y., & Chaiyen, P. (2020). Mechanistic insights into the dual activities of the single active site of l-lysine oxidase/monooxygenase from *Pseudomonas* sp. AIU 813. *Journal of Biological Chemistry*, 295(32), 11246-11261. <https://doi.org/https://doi.org/10.1074/jbc.RA120.014055>
71. Ullah, A. (2020). Structure-Function Studies and Mechanism of Action of Snake Venom L-Amino Acid Oxidases. *Front Pharmacol*, 11, 110. <https://doi.org/10.3389/fphar.2020.00110>
72. Valton, J., Filisetti, L., Fontcave, M., & Nivière, V. (2004). A Two-component Flavin-dependent Monooxygenase Involved in Actinorhodin Biosynthesis in *Streptomyces coelicolor**. *Journal of Biological Chemistry*, 279(43), 44362-44369. <https://doi.org/https://doi.org/10.1074/jbc.M407722200>
73. Wang, K., Zhao, L., Li, T., Wang, Q., Ding, Z., & Dong, W. (2023). Selective Immobilization of His-Tagged Enzyme on Ni-Chelated Ion Exchange Resin and Its Application in Protein Purification. *International Journal of Molecular Sciences*, 24(4), 3864. <https://www.mdpi.com/1422-0067/24/4/3864>
74. Wang, L., Jiao, B., Shen, Y., Du, R., Yuan, Q., & Wang, J. (2022). Co-Immobilization of Lactase and Glucose Isomerase on the Novel g-C(3)N(4)/CF Composite Carrier for Lactulose Production. *Nanomaterials (Basel)*, 12(23). <https://doi.org/10.3390/nano12234290>
75. Wicht, D. K. (2016). The reduced flavin-dependent monooxygenase SfnG converts dimethylsulfone to methanesulfinate. *Archives of Biochemistry and Biophysics*, 604, 159-166. <https://doi.org/10.1016/j.abb.2016.07.001>
76. Yan, F., Guo, X., Ye, Q., Li, P., Qi, J., & Wang, L. (2022). Removal of volatile dimethyl sulfoxide from wastewater using hydrogen peroxide catalyzed by supported molybdenum oxide. *Separation and Purification Technology*, 293, 121108. <https://doi.org/https://doi.org/10.1016/j.seppur.2022.121108>
77. Yu, X., Zhang, Z., Li, J., Su, Y., Gao, M., Jin, T., & Chen, G. (2021). Co-immobilization of multi-enzyme on reversibly soluble polymers in cascade catalysis for the one-pot

- conversion of gluconic acid from corn straw. *Bioresource Technology*, 321, 124509. <https://doi.org/https://doi.org/10.1016/j.biortech.2020.124509>
78. Zhan, X., Carpenter, R. A., & Ellis, H. R. (2008). Catalytic Importance of the Substrate Binding Order for the FMNH₂-Dependent Alkanesulfonate Monooxygenase Enzyme. *Biochemistry*, 47(7), 2221-2230. <https://doi.org/10.1021/bi701853w>
79. Zhang, F., Jin, J., Zhong, X., Li, S., Niu, J., Li, R., & Ma, J. (2011). Pd immobilized on amine-functionalized magnetite nanoparticles: a novel and highly active catalyst for hydrogenation and Heck reactions [10.1039/C0GC00854K]. *Green Chemistry*, 13(5), 1238-1243. <https://doi.org/10.1039/C0GC00854K>
80. Zhang, J., Dai, Y., Jiang, B., Zhang, T., & Chen, J. (2020). Dual-enzyme co-immobilization for the one-pot production of glucose 6-phosphate from maltodextrin. *Biochemical Engineering Journal*, 161, 107654. <https://doi.org/https://doi.org/10.1016/j.bej.2020.107654>
81. Zhao, M., Han, J., Wu, J., Li, Y., Zhou, Y., Wang, L., & Wang, Y. (2021). One-step separation and immobilization of his-tagged enzyme directly from cell lysis solution by biomimetic mineralization approach. *Biochemical Engineering Journal*, 167, 107893. <https://doi.org/https://doi.org/10.1016/j.bej.2020.107893>

VITA

NAME MONTISA MANGKALEE

DATE OF BIRTH 1 AUGUST 1995

PLACE OF BIRTH BANGKOK

INSTITUTIONS ATTENDED BSc Applied Chemistry (Chulalongkorn University)
MSc Pharmacology (King's college London)

HOME ADDRESS 799 Suksawad Rd. Bangpakok, Ratburana, Bangkok, Thailand
10140

